occupation of the invariant Vα14 receptor with α-GalCer on DC. The tonic expansion observed in the *in vitro* culture

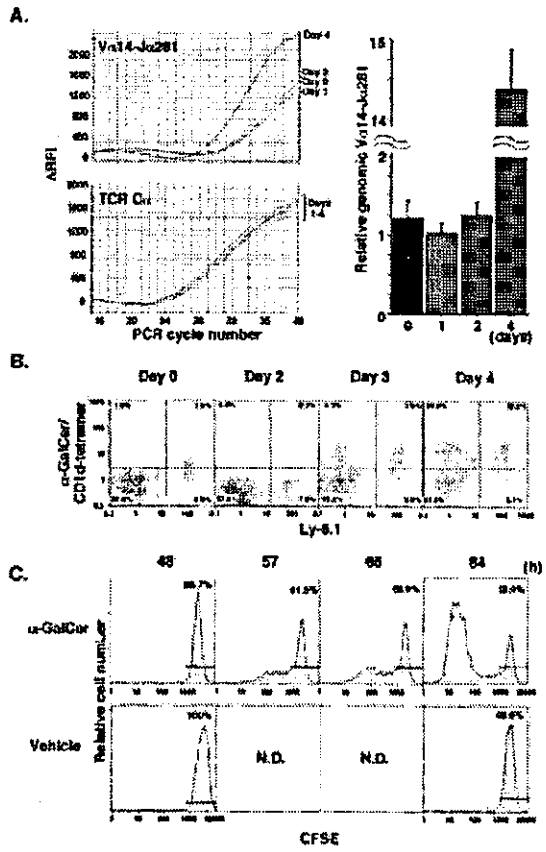

Fig. 3. Down-regulation of the invariant Vα14 receptor and survival of Vα14 NKT cells after α-GalCer stimulation. (A) Quantification of rearranged Vα14-Jα281 genomic DNA. The relative amounts of Vα14-Jα281 (left panel, upper) and TCR Cα (left panel, lower) genomic DNA from spleen cells stimulated with α-GalCer-DC were quantified by means of real-time PCR using Taqman probes. The amounts of rearranged Vα14–Jα281 genomic DNA were first compensated with that of TCR Cα and relative amounts of Vα14–Jα281 genes were calculated using an external standard prepared from Vα14 NKT hybridoma cells (data not shown). Relative amounts of genomic Vα14–Jα281 are plotted (right panel). Representative data from three independent experiments are shown with SD. (B) Study of Vα14 NKT cell destiny using Ly-5.1 and Ly-5.2 C57BL/6 mice. Electronically sorted liver Vα14 NKT cells from Ly-5.1 mice were mixed with spleen cells from Ly-5.2 mice at a ratio of 1:9 and co-cultured with α-GalCer-DC. The expression of the invariant Vα14 receptor was monitored with α-GalCer/CD1d tetramer. The percentage of cells in each subset is indicated. Representative data from two independent experiments are shown. (C) Cell division of Vα14 NKT cells after α-GalCer stimulation. Electronically sorted liver Vα14 NKT cells from Ly-5.2 mice were labeled with CFSE, mixed with Ly-5.1$^+$ spleen cells at a ratio of 1:9 and pulsed with α-GalCer or vehicle. The cell division of Ly-5.2$^+$ Vα14 NKT cells was monitored at the indicated time points after stimulation. Representative data from two independent experiments are shown. N.D. = not determined

(Fig. 2B), where there was no supply of Vα14 NKT cells, prompted us to hypothesize that α-GalCer/CD1d tetramer-reactive Vα14 NKT cells disappear, causing down-regulation of the Vα14 receptor, but are not eliminated.

To examine this hypothesis, we carried out a kinetic PCR analysis to rigorously measure the quantity of rearranged genomic Vα14–Jα281 upon receptor activation (Fig. 3A). When the relative numbers of Vα14–Jα281 genomic copies were compared after an appropriate compensations had been made using Cα, there was no change up to day 2, whereas the curve for the day 4 culture shifted to the left (equivalent to 3.5 PCR cycles). These results showed that there was no significant decrease in the number of Vα14–Jα281 genomic copies during the culture periods from day 0 to 2, implying that most of the Vα14 NKT cells were alive without significant cell death (Fig. 3A, left panel). The net increase in Vα14 NKT cell number upon stimulation was estimated to be in the range of 11-fold over 4 days (Fig. 3A, right panel).

The above data suggested that Vα14 NKT cells survive after stimulation rather than succumbing to death. To further explore this possibility, liver NK1.1$^+$ TCRβ$^+$ cells (of which >90% are α-GalCer/CD1d tetramer-reactive Vα14 NKT cells) from Ly-5.1 mice were purified by electronic cell sorting, mixed with Ly-5.2$^+$ spleen cells and stimulated with α-GalCer-DC. While Ly-5.1$^+$ Vα14 NKT cells expressed the invariant Vα14 receptor prior to stimulation, administration of α-GalCer-DC led to down-regulation of their invariant Vα14 receptor by day 2, resulting in a significant decrease in the number of Ly-5.1$^+$ Vα14 NKT cells (Fig. 3B, *cf.* day 0 and 2).

It is, however, of importance to note that the Ly-5.1$^+$ Vα14 NKT cells stayed alive even after α-GalCer-DC stimulation (Fig. 3B, day 0–4). As observed previously, α-GalCer/CD1d tetramer-reactive Vα14 NKT cells reappeared on day 3 (Fig. 3B, day 3) and the number of Ly-5.1$^+$ Vα14 NKT cells subsequently expanded to account for >18% of total cultured cells (Fig. 3B, day 4). These results clearly demonstrated that Ly-5.1$^+$ Vα14 NKT cells down-regulate their invariant Vα14 receptor upon α-GalCer stimulation, stay quiescent and eventually proliferate.

We also examined whether the observed cellular expansion accompanied cell division by labeling cells with CFSE. Electronically sorted liver NK1.1$^+$TCRβ$^+$ cells from Ly-5.2 mice were labeled with CFSE and mixed with unfractionated Ly-5.1$^+$ spleen cells. These mixtures were stimulated with α-GalCer or vehicle. It was not until 57 h after stimulation that cell division could be detected only in cells activated with α-GalCer (Fig. 3C, upper panel and data not shown). After that period, α-GalCer-stimulated cells continued to divide. In marked contrast, vehicle-stimulated Vα14 NKT cells showed little, if any, cell division (Fig. 3C, lower panel). These results indicated that α-GalCer promotes Vα14 NKT cell proliferation and further underpinned the above hypothesis.

Vα14 NKT cells are relatively resistant to apoptosis induced by receptor activation

The above data, however, did not exclude the possibility that a limited number of Vα14 NKT cells undergo apoptosis upon activation. We thus examined, by Annexin-V staining, whether Vα14 NKT cells underwent apoptosis upon stimulation. A comparison of Annexin-V staining upon anti-CD3 mAb stimu-

Reproduced with permission of the copyright owner. Further reproduction prohibited without permission.

lation showed less staining for Vα14 NKT cells relative to conventional T cells (TCRβ+NK1.1-) at all time points examined (Fig. 4A, left panel), suggesting that, albeit weakly, Vα14 NKT cells underwent apoptosis upon receptor-mediated activation. The number of cells that underwent apoptosis was further evaluated by measuring the amount of released DNA fragments by ELISA. As in the case of Annexin-V staining, fragmented DNA was observed in some fractions of Vα14 NKT cells, but the degree of fragmentation was less than that in conventional T cells (Fig. 4A, right panel).

To explore the molecular mechanisms underlying resistance to apoptosis in Vα14 NKT cells, we compared the profile of apoptosis-related gene expression in Vα14 NKT and conventional T cells through a DNA microarray study (Fig. 4B, upper panel and see Supplementary data). After stimulation with anti-CD3 mAb for 2 h, RNA was extracted from Vα14 NKT cells and from conventional T cells, and subjected to differential hybridization. To compare the signal intensity, we used scattered plot analysis (Array-Gage; Fuji Film). When the signal was normalized with HPRT, several molecules showed increased hybridization signal in Vα14 NKT cells relative to conventional T cells (Fig. 4B, upper and lower left panel). Subsequent semiquantitative RT-PCR analyses confirmed that NAIP and MyD118 were indeed up-regulated in Vα14 NKT cells relative to conventional T cells (Fig. 4B, lower right panel). We have also examined several genes that showed reduced expression in Vα14 NKT cells based on scattered plot data. It turned out that IL-1β, an indicator of apoptosis, showed reduced hybridization signal concomitant with decreased mRNA expression as revealed by RT-PCR analysis when compared to conventional T cells (Fig. 4B, lower panels) (12). All gene expression profiles in Vα14 NKT cells and in conventional T cells are available in the Supplementary data.

These differences in expression of apoptotic genes may reflect the intrinsic nature of each cell type. We also compared the expression of apoptosis-related genes in Vα14 NKT cells and conventional T cells prior to receptor activation. It was found that the expression profile of these cells prior to receptor activation mirrored that of post-receptor stimulation (*cf.* Fig. 4B, lanes 3 and 4, and C, lanes 1 and 2). Further kinetic studies on the expression of the indicated genes in Vα14 NKT cells *in vivo* revealed that, upon receptor activation, NAIP expression increased up to day 3, while expression thereafter gradually declined. MyD118 showed a similar expression pattern over time as NAIP, while the level of IL1-β expression remained constant (Fig. 4C).

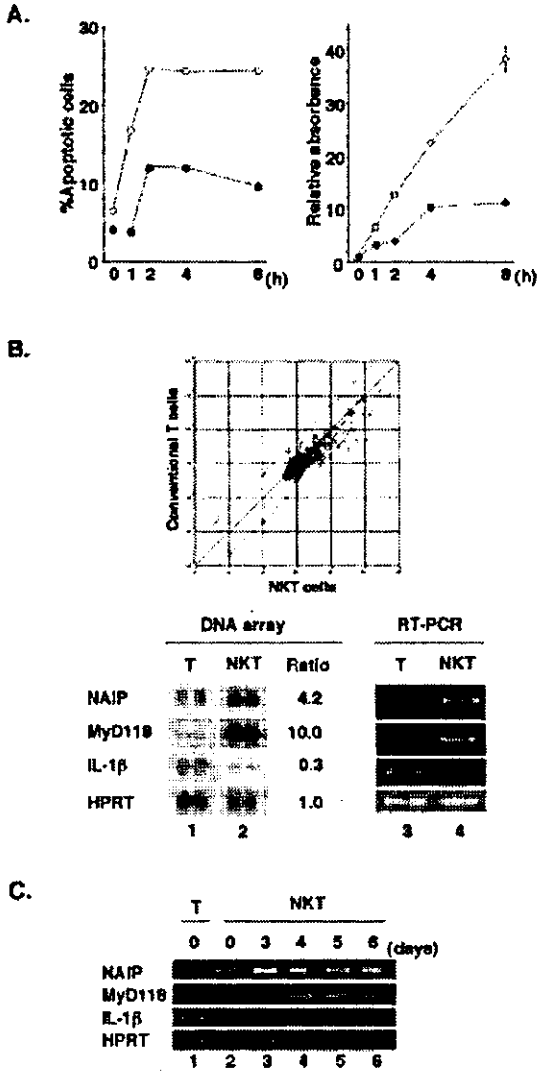

Fig. 4. Vα14 NKT cells are resistant to apoptotic cell death induced by receptor-mediated activation relative to conventional T cells. (A) Kinetics of apoptotic cell death induced by activation in Vα14 NKT cells and conventional T cells. Annexin-V expression levels were analyzed in electronically sorted Vα14 NKT cells and conventional T cells from the liver after stimulation with anti-CD3 mAb for the indicated periods of time. The percentage of Annexin-V-stained cells is shown as open circles for conventional T cells and closed circle for Vα14 NKT cells (left panel). Apoptosis was also quantified by measuring the amounts of fragmented DNA from the cells using an ELISA kit (right panel). Representative data from two independent experiments are shown. (B) Apoptosis-related genes are differentially expressed in Vα14 NKT cells stimulated for 2 h. Vα14 NKT cells and conventional T cells were isolated and stimulated as described in (A). Total RNA was extracted and subjected to RNA amplification. After random priming, differential hybridization was performed. Upper panel: scattered plot analysis between NKT and conventional T cells. Lower left panel: differential hybridization signal on DNA array. The ratio represents the fold change of the hybridization signal between two groups in duplicate experiments after normalizing with the signal of HPRT. Lower right panel: RT-PCR detection for NAIP, MyD118 and IL-1β in cells used for DNA array experiments. HPRT serves as a control to assure the equal amount of the recovered RNA. (C) Up-regulation of anti-apoptotic genes upon receptor activation *in vivo*. After *in vivo* stimulation with α-GalCer for the indicated periods of time, NKT cells from the spleen were electronically sorted. RNA was extracted from spleen NKT cells at the indicated time, and subjected to RT-PCR with primers for NAIP, MyD118 and IL-1β. HPRT serves as control to ensure equal cDNA input in each lane. For comparison, RNA from the same number of conventional spleen T cells was subjected to RT-PCR without any stimulation.

Reproduced with permission of the copyright owner. Further reproduction prohibited without permission.

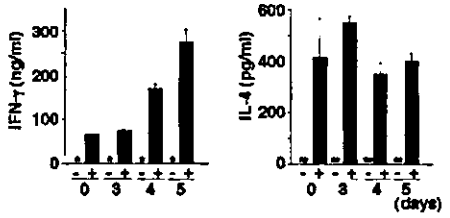

Fig. 5. Cytokine production from re-stimulated Vα14 NKT cells. Total spleen cells were cultured in the presence of α-GalCer-DC as described in Fig. 2(B) for the indicated periods of time (day 0–5). Cells were then collected, washed and stimulated with vehicle-DC (–) or re-stimulated with α-GalCer-DC (+) for another 72 h. The concentration of IFN-γ and IL-4 in the supernatant was determined by ELISA. Data from three independent experiments are shown with ± SD. The asterisks (* and **) indicate that the concentration was below the detection threshold for IFN-γ (<0.16 ng/ml) or IL-4 (<15.6 pg/ml), respectively.

Vα14 NKT cell resistance to tolerance induction after receptor down-regulation

Since the activation of T cells often results in the loss of their function and becomes tolerant (2), the ability of Vα14 NKT cells to secrete IFN-γ and IL-4 upon re-stimulation with α-GalCer-DC or vehicle-DC was examined at the indicated time points following the initial α-GalCer-DC stimulation. At any given time point, even after the down-regulation of the Vα14 receptor, activated Vα14 NKT cells produced both IFN-γ and IL-4 upon re-stimulation with α-GalCer-DC (Fig. 5). In contrast, neither IFN-γ nor IL-4 production could be observed following vehicle-DC re-stimulation (Fig. 5). These results indicate that the activation of Vα14 NKT cells does not affect cytokine production in these cells after re-stimulation.

Discussion

We have demonstrated that Vα14 NKT cell activation results in the subsequent down-regulation of the Vα14 receptor. Activated Vα14 NKT cells remain quiescent for a while, but eventually proliferate. However, the effector functions of activated Vα14 NKT cells, such as cytokine production, remain intact even after receptor down-regulation. These unique features distinguish Vα14 NKT cells from other types of effector T cells which are readily subjected to clonal deletion or anergy upon TCR-mediated activation.

Our present data are somewhat contradictory to the previous reports claiming that NKT cells, defined as NK1.1$^+$TCRβ^{dim} cells, are extremely sensitive to IL-12- and TCR-induced apoptosis (13). This is most evident in our *in vitro* experiments where there is no provision of exogenous Vα14 NKT cells or Vα14 NKT cell progenitors (Fig. 2B). Under such conditions, the rapid disappearance and subsequent expansion of Vα14 NKT cells upon α-GalCer challenge cannot be attributed to the immediate eradication of the cells by apoptosis. Rather, the seeming disappearance of Vα14 NKT cells is better explained by the down-regulation of the Vα14 receptor. This interpretation is further supported by transfer experiments using Ly-5.1$^+$ cells and by kinetic PCR (Fig. 3). Still, more detailed studies are needed to elucidate the precise mechanism of Vα14 NKT cell number reduction following receptor stimulation *in vivo* (Figs 1 and 2A). Apoptotic cell death may play a role in this process. However, since the expression of certain anti-apoptotic genes is up-regulated following receptor activation, it appears likely that NKT cells become less susceptible to apoptosis over time (see below, Fig. 4C).

The molecular mechanism underlying the resistance of Vα14 NKT cells to TCR-mediated apoptosis was further explored by DNA microarray studies combined with RT-PCR analysis (Fig. 4B). Our results indicate that the resistance to apoptosis of Vα14 NKT cells relative to conventional T cells is primarily due to the preferential expression of anti-apoptotic genes, such as NAIP and MyD118. NAIP belongs to the inhibitor of apoptosis (IAP) that regulates lymphocyte sensitivity to Fas-mediated apoptosis (3,14). IAP bind activated caspases, and target their ubiquitination and degradation via the baculovirus IAP repeat (BIR) motif, which eventually allows the cells to survive upon Fas-induced signals. MyD118, also known as Gadd45β, was first identified as a member of the Gadd45 family associated with cell-cycle control and DNA repair (15,16). MyD118/Gadd45β is induced by an apoptotic factor, tumor necrosis factor-α, and acts as an anti-apoptotic protein by inhibiting JNK activity (17). Since continuous activation of JNK activity is tightly correlated with apoptosis (18), its inhibition results in the blocking of apoptosis. In summary, the increased expression of anti-apoptotic genes post-receptor activation together with the unaltered expression of IL-1β in Vα14 NKT cells may explain, at least in part, why these cells are more resistant to apoptosis than conventional T cells. In the light of these data, it is not surprising that Vα14 NKT cells are relatively resistant to apoptosis induced by irradiation and glucocorticoid treatment (19,20). Since conventional T cells comprise naive and memory cells, a more fine comparison in the expression of anti-apoptotic genes between Vα14 NKT cells and conventional T cells will provide more insight into the anti-apoptotic mechanism in Vα14 NKT cells.

Another unique facet of Vα14 NKT cells is that its effector function, the production of cytokines, is kept intact even after activation (Fig. 5). This indicates that Vα14 NKT cells do not become anergic upon receptor activation. In line with this, priming α-GalCer-pulsed DC *in vivo* followed by re-stimulation with α-GalCer-pulsed DC *in vitro* does not induce anergy in Vα14 NKT cells (21). However, we have to mention that the amount of IL-4 produced by activated NKT cells was relatively constant regardless of the different NKT cell number (Figs 2A and 5). This may be explained, at least in part, by the fact that IL-4 produced from the activated NKT cells is consumed by NKT cells *per se* or B cells, thus culminating in the similar net production of IL-4 (22,23).

These distinct features of Vα14 NKT cells may be tightly linked to the role of Vα14 NKT cells in controlling and suppressing autoreactive effector T cells. Collectively, it is conceivable that the nature of Vα14 NKT cells to be resistance to tolerance induction as well as apoptosis after down-regulation of the invariant Vα14 receptor confers on these cells the ability to mediate a long-lasting regulatory function under any given circumstances.

These findings will open the door to the elucidation of the homeostasis of immunoregulatory cells.

Reproduced with permission of the copyright owner. Further reproduction prohibited without permission.

Acknowledgements

The authors thank Ms Hiroko Tanabe for the preparation of this manuscript and Kirin Brewery Co. Ltd for support of this study. This work was in part supported by grants from the Ministry of Education, Culture, Sports, Science and Technology (Japan) through a grant under the Special Coordination Fund for the Promotion of Science and Technology (T. N.), and through Grants-in-Aid for Scientific Research C#13218016 (T. N.), A#13307011 (M. T.), B#14370107 (T. N.) and C#12670293 (T. N.); the Program for the Promotion of Fundamental Studies in Health Sciences, Organization for Pharmaceutical Safety and Research, Ministry of Health, Labor and Welfare (M. T.); and the Human Frontier Science Program, RG00168/2000-M206 (M. T).

Abbreviations

α-GalCer	α-galactosylceramide
CFSE	carboxyfluorescein diacetate succinimidyl ester
DC	dendritic cell
IAP	inhibitor of apoptosis

References

1 Lenardo, M., Chan, K. M., Hornung, F., McFarland, H., Siegel, R., Wang, J. and Zheng, L. 1999. Mature T lymphocyte apoptosis-immune regulation in a dynamic and unpredictable antigenic environment. *Annu. Rev. Immunol.* 17:221.

2 Schwartz, R. H. 2003. T cell anergy. *Annu. Rev. Immunol.* 21:305.

3 Rathmell, J. C. and Thompson, C. B. 2002. Pathways of apoptosis in lymphocyte development, homeostasis, and disease. *Cell* 109(Suppl.):S97.

4 Banz, A., Pontoux, C. and Papiernik, M. 2002. Modulation of Fas-dependent apoptosis: a dynamic process controlling both the persistence and death of CD4 regulatory T cells and effector T cells. *J. Immunol.* 169:750.

5 Takahashi, T., Tagami, T., Yamazaki, S., Uede, T., Shimizu, J., Sakaguchi, N., Mak, T. W. and Sakaguchi, S. 2000. Immunologic self-tolerance maintained by CD25$^+$CD4$^+$ regulatory T cells constitutively expressing cytotoxic T lymphocyte-associated antigen 4. *J. Exp. Med.* 192:303.

6 Shevach, E. M. 2002. CD4$^+$CD25$^+$ suppressor T cells: more questions than answers. *Nat. Rev. Immunol.* 2:389.

7 Lantz, O. and Bendelac, A. 1994. An invariant T cell receptor alpha chain is used by a unique subset of major histocompatibility complex class I-specific CD4$^+$ and CD4$^-$8$^-$ T cells in mice and humans. *J. Exp. Med.* 180:1097.

8 Bendelac, A., Lantz, O., Quimby, M. E., Yewdell, J. W., Bennink, J. R. and Brutkiewicz, R. R. 1995. CD1 recognition by mouse NK1$^+$ T lymphocytes. *Science* 268:863.

9 Cui, J., Shin, T., Kawano, T., Sato, H., Kondo, E., Toura, I., Kaneko, Y., Koseki, H., Kanno, M. and Taniguchi, M. 1997. Requirement for Vα14 NKT cells in IL-12-mediated rejection of tumors. *Science* 278:1623.

10 Kawano, T., Cui, J., Koezuka, Y., Toura, I., Kaneko, Y., Motoki, K., Ueno, H., Nakagawa, R., Sato, H., Kondo, E., Koseki, H. and Taniguchi, M. 1997. CD1d-restricted and TCR-mediated activation of Vα14 NKT cells by glycosylceramides. *Science* 278:1626.

11 Taniguchi, M., Harada, M., Kojo, S., Nakayama, T. and Wakao, H. 2003. The regulatory role of Vα14 NKT cells in innate and acquired immune response. *Annu. Rev. Immunol.* 21:483.

12 Rathmell, J. C. and Thompson, C. B. 1999. The central effectors of cell death in the immune system. *Annu. Rev. Immunol.* 17:781.

13 Eberl, G. and MacDonald, H. R. 1998. Rapid death and regeneration of NKT cells in anti-CD3ε- or IL-12-treated mice: a major role for bone marrow in NKT cell homeostasis. *Immunity* 9:345.

14 Gotz, R., Karch, C., Digby, M. R., Troppmair, J., Rapp, U. R. and Sendtner, M. 2000. The neuronal apoptosis inhibitory protein suppresses neuronal differentiation and apoptosis in PC12 cells. *Hum. Mol. Genet.* 9:2479.

15 Wang, X. W., Zhan, Q., Coursen, J. D., Khan, M. A., Kontny, H. U., Yu, L., Hollander, M. C., O'Connor, P. M., Fornace, A. J., Jr and Harris, C. C. 1999. GADD45 induction of a G_2/M cell cycle checkpoint. *Proc. Natl Acad. Sci. USA* 96:3706.

16 Zhan, Q., Antinore, M. J., Wang, X. W., Carrier, F., Smith, M. L., Harris, C. C. and Fornace, A. J., Jr. 1999. Association with Cdc2 and inhibition of Cdc2/Cyclin B1 kinase activity by the p53-regulated protein Gadd45. *Oncogene* 18:2892.

17 De Smaele, E., Zazzeroni, F., Papa, S., Nguyen, D. U., Jin, R., Jones, J., Cong, R. and Franzoso, G. 2001. Induction of gadd45β by NF-κB downregulates pro-apoptotic JNK signalling. *Nature* 414:308.

18 Chen, Y. R. and Tan, T. H. 2000. The c-Jun N-terminal kinase pathway and apoptotic signaling. *Int. J. Oncol.* 16:651.

19 Kimura, M., Watanabe, H., Ohtsuka, K., Iiai, T., Tsuchida, M., Sato, S. and Abo, T. 1993. Radioresistance of intermediate TCR cells and their localization in the body of mice revealed by irradiation. *Microbiol. Immunol.* 37:641.

20 Tamada, K., Harada, M., Abe, K., Li, T. and Nomoto, K. 1998. IL-4-producing NK1.1$^+$ T cells are resistant to glucocorticoid-induced apoptosis: implications for the T_h1/T_h2 balance. *J. Immunol.* 161:1239.

21 Fujii, S., Shimizu, K., Kronenberg, M. and Steinman, R. M. 2002. Prolonged IFN-γ-producing NKT response induced with α-galactosylceramide-loaded DCs. *Nat. Immunol.* 3:867.

22 Kaneko, Y., Harada, M., Kawano, T., Yamashita, M., Shibata, Y., Gejyo, F., Nakayama, T. and Taniguchi, M. 2000. Augmentation of Vα14 NKT cell-mediated cytotoxicity by interleukin 4 in an autocrine mechanism resulting in the development of concanavalin A-induced hepatitis. *J. Exp. Med.* 191:105.

23 Yoshimoto, T., Min, B., Sugimoto, T., Hayashi, N., Ishikawa, Y., Sasaki, Y., Hata, H., Takeda, K., Okumura, K., Van Kaer, L., Paul, W. E. and Nakanishi, K. 2003. Nonredundant roles for CD1d-restricted natural killer T cells and conventional CD4$^-$ T cells in the induction of immunoglobulin E antibodies in response to interleukin 18 treatment of mice. *J. Exp. Med.* 197:997.

Reproduced with permission of the copyright owner. Further reproduction prohibited without permission.

Genetic Alterations in Early-Stage Pulmonary Large Cell Neuroendocrine Carcinoma

Kenzo Hiroshima, M.D.[1]
Akira Iyoda, M.D.[2]
Kiyoshi Shibuya, M.D.[2]
Yukiko Haga, M.D.[2]
Tetsuya Toyozaki, M.D.[1]
Toshihiko Iizasa, M.D.[2]
Toshinori Nakayama, M.D.[3]
Takehiko Fujisawa, M.D.[2]
Hidemi Ohwada, M.D.[1]

[1] Department of Basic Pathology, Graduate School of Medicine, Chiba University, Chiba, Japan.

[2] Department of Thoracic Surgery, Graduate School of Medicine, Chiba University, Chiba, Japan.

[3] Department of Medical Immunology, Graduate School of Medicine, Chiba University, Chiba, Japan.

Supported in part by the Smoking Research Foundation.

The authors thank Ms. Ayaka Sato, Ms. Tamiyo Taniguchi, Ms. Tomoko Sakai, and Ms. Kazuko Abe for their technical assistance.

Address for reprints: Kenzo Hiroshima, M.D., Department of Basic Pathology, Graduate School of Medicine, Chiba University, 1-8-1 Inohana, Chuo-ku, Chiba, Chiba, 260-8670 Japan; Fax: (011) 81-43-226-2180; E-mail: kenzo@faculty.chiba-u.jp

Received August 29, 2003; revision received November 24, 2003; accepted January 5, 2004.

© 2004 American Cancer Society
DOI 10.1002/cncr.20108

BACKGROUND. Small cell lung carcinoma (SCLC) and pulmonary large cell neuroendocrine carcinoma (LCNEC) are high-grade malignant neuroendocrine tumors. Histologic differentiation between SCLC and LCNEC is difficult in some cases and to the authors' knowledge, genetic alterations associated with LCNEC have not been identified. Therefore, the authors studied genetic alterations found in LCNEC and compared them with those of SCLC and classic large cell carcinoma (CLCC).

METHODS. Twenty-two patients with UICC TNM Stage I LCNEC, 12 patients with Stage I CLCC, and 11 patients with SCLC with limited disease were studied. All tumors were resected completely. Loss of heterozygosity (LOH) of the tumor cells was detected using fluorescent primers. Methylation status of the p16 gene and expression of the p53 protein, retinoblastoma protein, and p16 protein were evaluated immunohistochemically.

RESULTS. LOH at TP53 and 13q14 was observed in most patients. The prevalence of LOH at D3S1295, D3S1234, and D5S407 was significantly higher in patients with LCNEC and SCLC than in patients with CLCC. The prevalence of LOH at D5S422 was higher in patients with CLCC and in patients with SCLC than in patients with LCNEC. Expression of the p16 protein was observed more frequently in SCLC than in CLCC or LCNEC. Hypermethylation of the p16 gene was observed more frequently in LCNEC than in SCLC. Patients with allelic losses at D3S1234 and D10S1686 had poorer prognoses compared with patients without allelic losses at these sites.

CONCLUSIONS. Genetic alterations of LCNEC were akin to those of SCLC. However, allelic losses at 5q and abnormalities in the p16 gene may differentiate LCNEC from SCLC. *Cancer* 2004;100:1190–8. © *2004 American Cancer Society.*

KEYWORDS: lung, large cell neuroendocrine carcinoma, small cell carcinoma, loss of heterozygosity, methylation, p16, p53, retinoblastoma protein.

In 1999, the World Health Organization (WHO) reclassified large cell carcinomas into four types based on neuroendocrine morphology by light microscopy and neuroendocrine differentiation by immunohistochemistry or electron microscopy.[1] These four types were large cell neuroendocrine carcinoma (LCNEC), large cell carcinoma with neuroendocrine differentiation (LCCND), large cell carcinoma with neuroendocrine morphology (LCCNM), and classic large cell carcinoma (CLCC). LCNEC has both neuroendocrine morphology and differentiation, as shown by electron microscopy and/or immunohistochemistry; LCCND lacks neuroendocrine morphology but has neuroendocrine markers, as observed by electron microscopy and/or immunohistochemistry; LCCNM has neuroendocrine morphologic features but lacks neuroendocrine markers, as observed by electron microscopy and/or immunohistochemistry; and CLCC lacks neu-

roendocrine morphology or differentiation, as indicated by special studies.

We found that large cell carcinomas with neuroendocrine features (LCNF), including LCNEC, LCCND, and LCCNM, appear to be more clinically aggressive tumors than CLCC.[2] Although the WHO classified the neuroendocrine tumors into typical carcinoid, atypical carcinoid, LCNEC, and small cell lung carcinoma (SCLC), the differentiation between LCNEC and SCLC is difficult in some cases.[3,4] Previous studies of lung carcinomas have shown allele deletions using a variety of methods.[5,6] However, to our knowledge, no comparative allelotyping of SCLC and LCNEC has been reported. The aims of the current study were to elucidate the genetic changes in patients with LCNEC and compare them with patients with CLCC and with SCLC.

MATERIALS AND METHODS

Tumor Specimens

Tumor staging was performed using the TNM criteria of the International Union Against Cancer (UICC). We analyzed 22 patients with Stage I LCNEC (T1N0M0 or T2N0M0). This type of tumor does not invade adjacent organs (T1 or T2) and has no regional lymph node metastasis (N0) and no distant metastasis (M0). We also analyzed 12 patients with Stage I CLCC and 11 patients with SCLC with limited disease who underwent surgical resection at Chiba University Hospital between 1987 and 1999. All tumors were resected completely. We performed immunohistochemical staining for all LCNECs and all CLCCs. Neuroendocrine differentiation was detected by positive immunohistochemical staining for anti-chromogranin A antibody, anti-synaptophysin antibody, or antineural cell adhesion molecule (NCAM) antibody. We confirmed a lack of neuroendocrine differentiation in all CLCCs. Tumor specimens were classified according to the WHO classification system for lung carcinoma by two experienced pulmonary pathologists (K.H. and H.O.). Each pathologist classified the tumor specimens independently and unanimous agreement was obtained. In addition, four patients with LCNEC and three patients with SCLC were included in the current study to evaluate whether there was expression of the p53, retinoblastoma (Rb), and p16 proteins using immunohistochemical methods. To evaluate hypermethylation of the p16 gene, two patients with SCLC were added to the study. Informed consent was obtained from all patients.

One of the 26 patients with LCNEC underwent preoperative radiotherapy, whereas 1 of 12 with CLCC and 7 of 14 with SCLC underwent preoperative chemotherapy. Seven patients with LCNEC, 1 patient with CLCC, and 10 patients with SCLC underwent postoperative adjuvant chemotherapy, whereas 1 patient with LCNEC and 1 patient with SCLC underwent postoperative radiotherapy.

Microdissection and DNA Extraction

DNA samples were extracted from paraffin-embedded materials. Tissue specimens were accurately removed from four 10-μm serial sections mounted on glass slides by scraping the marked area with a needle under a stereomicroscope. Tumor cells were selectively removed from the sections to minimize contamination by normal tissue specimens. The dissected sections were digested by proteinase K over 2 nights at 37 °C. After phenol/chloroform extraction, DNA samples were precipitated with cold ethanol overnight at −20 °C and centrifuged. The dried pellets were then resuspended in 50 μl Tris-ethylenediamine tetraacetic acid buffer (Tris-EDTA).

Polymorphic DNA Markers and Polymerase Chain Reaction–Loss of Heterozygosity

To evaluate loss of heterozygosity (LOH), 13 microsatellite markers were used: D3S1234 (3p14.2), D3S1481 (3p14.2), D3S1295 (3p21.1), D3S1581 (3p21.3), D5S407 (5q11), D5S410 (5q31.3), D5S422 (5q33), D9S171 (9p21), IFNA (9p22), D10S249 (10p15.3), D10S1686 (10q22.3), D13S153 (13q14), and ALE3/P53ivs1b(TP53). The forward primers were labeled at the 5′ end with the fluorochromes 6-FAM (blue), VIC (green), or NED (yellow).

Polymerase chain reaction (PCR) was performed with a PCR thermal cycler MP (Takara, Otsu, Japan). The PCR reactions were comprised of 2.5 mmol/L deoxynucleotide triphosphates, 40 pmol/L each primer, 1.25 U Gene Taq (Nippon Gene, Toyama, Japan), 20 mmol/L Tris-HCl (pH 8.0), and 15 mmol/L $MgCl_2$. The PCR program was comprised of a denaturation cycle at 95 °C for 5 minutes and 85 °C for 3 minutes (to allow for the addition of Gene Taq), followed by 40 cycles of 95 °C for 30 seconds, 55–60 °C for 30 seconds, 72 °C for 30 seconds, and 72 °C for 10 minutes.

The loading mix was prepared with 12 μl of deionized formamide, 0.4 μl GeneScan internal lane size standard (Applied Biosystems, Foster City, CA), and 6-FAM, VIC, or NED-labeled PCR products that were prediluted with water. Samples were denatured for 5 minutes at 95 °C, then cooled by placing directly on ice and loaded onto the ABI Prism 3100 genetic analyzer (Applied Biosystems). The fluorescent bands were laser scanned and the data were stored electronically. The data were processed using the software package ABI GeneScan (Applied Biosystems). LOH was defined

as a reduction of the peak height of an allele by ≥ 50% in the tumor, compared with the normal sample.

Calculation of Fractional Regional Loss Index

The fractional regional loss (FRL) index was calculated as follows: FRL index = (total number of chromosomal regions with LOH)/(total number of informative regions).

Methylation Analysis

The methylation state of the p16 gene was evaluated by methylation-specific PCR as previously reported.[7] Briefly, genomic DNA samples are modified by treatment with sodium bisulfite, which converts all unmethylated cytosines to uracil, then to thymidine during the subsequent PCR step. DNA samples are then purified using Wizard DNA purification resin (Promega, Madison, WI), desulfonated with NaOH, precipitated with ethanol, and finally suspended in a Tris-EDTA buffer. Two sets of primers are used to amplify each region of interest. One pair recognizes a sequence in which CpG sites are unmethylated (bisulfite modified to UpG) and the other pair recognizes a sequence in which CpG sites are methylated (unmodified by bisulfite). PCR amplification was performed using 60 ng of treated DNA samples as the template. Forty cycles of amplification were used in the analysis of modified DNA samples. PCR products were loaded onto 4.0% agarose gels, stained with ethidium bromide, and visualized under ultraviolet illumination.

Immunohistochemistry

All tumor specimens were evaluated by immunohistochemical staining. Four-micrometer sections were cut from formalin-fixed, paraffin-embedded tissue specimens and placed on silanized slides (Dakopatts, Glostrup, Denmark). They were stained with polyclonal anti-chromogranin A antibody (prediluted) (Nichirei, Tokyo, Japan), polyclonal anti-synaptophysin antibody (prediluted; Dakopatts), monoclonal anti-NCAM antibody (prediluted) (Zymed, San Francisco, CA), monoclonal antibody (MoAb) DO-7 (1:800; Dakopatts), which reacts with both wild-type and mutant p53 protein, monoclonal anti-p16 protein antibody (1:50; Pharmingen, San Diego, CA), and monoclonal anti-Rb protein antibody (1:50; Pharmingen).

A Histofine simple stain kit (Nichirei) was used for immunostaining. To improve the staining pattern, the tissue specimens were pretreated by microwaving for 15 minutes in citrate buffer (10 mmol/L, pH 6.0) before staining with anti-NCAM antibody, DO-7, anti-p16 protein antibody, and anti-Rb protein antibody, or by autoclaving at 121 °C for 15 minutes before staining with anti-synaptophysin antibody. DO-7 immunoreactivity was classified as positive when the proportion of positively stained cells was > 10% of all tumor cells. Rb and p16 protein immunoreactivity was classified as positive when the nuclei of the cells were stained.

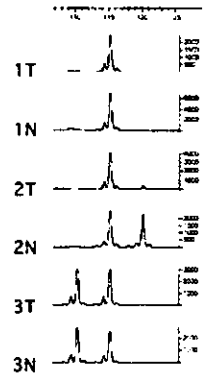

FIGURE 1. GeneScan results of microsatellite analysis using ALE3/P53ivs1b. The fluorescence of one peak was observed at base pair (bp) 115, both in the amplified product derived from the DNA samples retrieved from tumor (1T) and normal (1N; homozygous) specimens. The fluorescence signals of two peaks were observed at bp 115 and 120 in the amplified product derived from the DNA sample of 2N. However, the fluorescence of 1 peak at bp 120 was decreased in 2T (loss of heterozygosity). The fluorescence signals of two peaks at bp 110 and 115 were observed in the amplified product derived from the DNA samples of 3T and 3N (heterozygous).

Survival Analysis

The length of disease-free survival was defined as the interval between the date of surgery and the time of first local or distant disease recurrence. This was evaluated using the method of Kaplan and Meier.[8] The curves obtained were compared with the log-rank test results.

Statistical Analysis

The Fisher exact test was used to evaluate the prevalence of LOH, methylation status, and the immunohistochemistry results for the various lung carcinoma subtypes. Differences in FRL indices among the three types of lung carcinoma were tested by the Mann–Whitney U test. Probability values of $P < 0.05$ were regarded as statistically significant.

RESULTS

Microsatellite Analysis

Representative results are shown in Figures 1 and 2 and a summary of the analysis is shown in Table 1. Allelic losses at TP53 and at 13q14 were frequent in the three types of lung carcinoma analyzed in the current

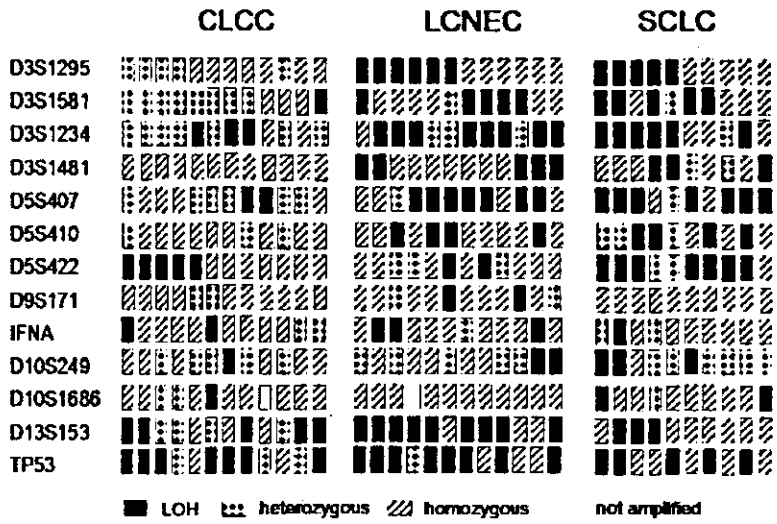

FIGURE 2. Schematic representation of the deletion map for the tumors studied.

TABLE 1
Rates of Allelic Loss among Lung Carcinomas Related to Chromosomal Regions and Markers

Markers	Region	CLCC	LCNEC	SCLC	*P* values for CLCC and LCNEC	*P* values for CLCC and SCLC
D3S1234	3p14.2	3/10 (30.0)	12/18 (66.7)	7/8 (87.5)	0.0426[a]	0.0248[b]
D3S1481	3p14.2	0/0	9/11 (81.8)	3/5 (60.0)		
D3S1295	3p21.1	0/5 (0)	9/10 (90.0)	5/5 (100)	0.0020[a]	0.0079[b]
D3S1581	3p21.3	1/9 (11.1)	6/11 (54.5)	5/7 (71.4)		0.0350[b]
	any 3p	4/10 (40.0)	20/21 (95.2)	10/11 (90.9)	0.0017[a]	0.0237[b]
D5S407	5q11	2/8 (25.0)	12/16 (75.0)	8/9 (88.9)	0.0324[a]	0.0152[b]
D5S422	5q33	5/5 (100)	3/10 (30.0)	8/10 (80.0)	0.0256[a]	
D5S410	5q31.3	0/3 (0)	5/7 (71.4)	4/7 (57.1)		
D9S171	9p21	0/2 (0)	2/6 (33.3)	0/0		
IFNA	9p22	2/4 (50.0)	4/9 (44.4)	1/4 (25.0)		
D10S249	10p15.3	1/6 (16.7)	6/14 (42.9)	4/10 (40.0)		
D10S1686	10q22.3	1/3 (33.3)	1/2 (50.0)	2/3 (66.7)		
D13S153	13q14	5/9 (55.6)	11/13 (84.6)	3/3 (100)		
ALE3/P53ivs1b	TP53	7/10 (70.0)	10/14 (71.4)	6/6 (100)		

CLCC: classic large cell carcinoma; LCNEC: large cell neuroendocrine carcinoma; SCLC: small cell lung carcinoma.
[a] Statistically significant difference between CLCC and LCNEC.
[b] Statistically significant difference between CLCC and SCLC.

study. Allelic losses at D3S1295 were more frequent in LCNEC and in SCLC than in CLCC. The difference in frequency between SCLC and CLCC and between LCNEC and CLCC was statistically significant ($P = 0.0079$ and $P = 0.0020$, respectively). Allelic losses at D3S1234 were more frequent in LCNEC and in SCLC than in CLCC. The difference in frequency between SCLC and CLCC and between LCNEC and CLCC was statistically significant ($P = 0.0248$ and $P = 0.0426$, respectively). Allelic losses at D3S1581 were more frequent in SCLC than in CLCC and the difference was statistically significant ($P = 0.0350$). Allelic losses at D5S407 were also more frequent in LCNEC and in SCLC than in CLCC. The difference in frequency between SCLC and CLCC and between LCNEC and CLCC was statistically significant ($P = 0.0152$ and $P = 0.0324$, respectively). Allelic losses at D5S422 were more frequent in CLCC and in SCLC than in LCNEC. The difference in frequency between CLCC and LCNEC was statistically significant ($P = 0.0256$).

LOH was observed frequently in one or more of the microsatellite markers on 3p in LCNEC and SCLC. Allelic losses at one or more of the microsatellite markers on 3p were observed in 20 of 21 informative

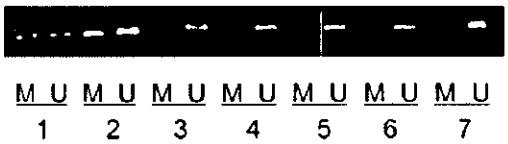

FIGURE 3. Methylation-specific polymerase chain reaction (PCR) of the p16 gene. The presence of visible PCR product in Lanes U and M indicates the presence of unmethylated and methylated genes, respectively. (Lanes 1–4) Large cell neuroendocrine carcinoma. (Lanes 5, 6) Classic large cell carcinoma. (Lane 7) Small cell carcinoma.

cases of LCNEC (95.2%), 10 of 11 informative cases of SCLC (90.9%), and 4 of 10 informative cases of CLCC (40%). The difference in frequency between SCLC and CLCC and between LCNEC and CLCC was statistically significant ($P = 0.0237$ and $P = 0.0017$, respectively). However, the difference between LCNEC and SCLC was not statistically significant.

The FRL index was used to compare the overall LOH frequencies. The mean FRL was higher in SCLC (0.74) and in LCNEC (0.62) than in CLCC (0.38). The differences between CLCC and LCNEC, and between CLCC and SCLC, were statistically significant ($P = 0.0031$ and $P = 0.0015$, respectively), but the difference between LCNEC and SCLC was not significant ($P = 0.1941$). The mean FRL of 3p was higher in SCLC (0.84) and in LCNEC (0.75) than in CLCC (0.20). The differences between CLCC and LCNEC, and between CLCC and SCLC, were statistically significant ($P = 0.0010$ and $P = 0.0012$, respectively), but the difference between LCNEC and SCLC was not significant ($P = 0.4275$).

Hypermethylation of the p16 Gene

Representative results are shown in Figure 3. Hypermethylation of the p16 gene was observed in 4 of 12 informative cases of CLCC (33.3%), in 7 of 18 informative cases of LCNEC (38.9%), and in none of the 12 informative cases of SCLC (0%). There was a statistically significant difference in the frequency of hypermethylation of the p16 gene between LCNEC and SCLC ($P = 0.0242$).

Immunohistochemistry

Because the p53, Rb, and p16 proteins are nuclear molecules, only nuclear activity was recorded in the current study. Expression of these proteins was evaluated by staining with the MoAbs DO-7, anti-Rb, and anti-p16, respectively. Normal lung tissue specimens generally showed negative nuclear staining for the p53, Rb, and p16 proteins. A summary of the results is shown in Table 2. The frequency of p16 expression

TABLE 2
Summary of Immunohistochemical Staining Results

Characteristics	CLCC	LCNEC	SCLC	*P* values
Rb				
Positive	5	9	1	
Negative	7	17	13	
p16				
Positive	4	15	13	0.0029[a]
Negative	8	11	1	0.0301[b]
DO7				
Positive	6	15	11	
Negative	6	11	3	

CLCC: classic large cell carcinoma; LCNEC: large cell neuroendocrine carcinoma; SCLC: small cell lung carcinoma.
[a] Statistically significant difference between CLCC and SCLC.
[b] Statistically significant difference between LCNEC and SCLC.

was significantly higher in SCLC than in CLCC ($P = 0.0029$) and in LCNEC ($P = 0.0301$). The difference between LCNEC and CLCC was not statistically significant. In SCLC, methylation of the p16 gene was not observed and the p16 protein was expressed in all but one patient. Of 11 nonsmall cell lung carcinomas (NSCLCs) harboring hypermethylation of the p16 gene, 9 showed an absence or lowering of protein expression and two showed highly positive staining for the p16 protein.

p16-negative lung carcinomas tended to express Rb protein, whereas p16-positive lung carcinomas did not. Staining of tumors with anti-p16 MoAb correlated with staining of the tumor with anti-Rb MoAb ($P < 0.0001$). All patients with SCLCs, except one, expressed p16 protein but not Rb protein. One SCLC was accompanied by a squamous cell carcinoma. Most of the tumor specimen was a squamous cell carcinoma and approximately 10% of the tumor specimen showed the characteristics of SCLC. The SCLC component stained with anti-p16 MoAb but not with anti-Rb MoAb, whereas the squamous cell carcinoma component stained with anti-Rb MoAb but not with anti-p16 MoAb (Fig. 4).

Survival Analysis

The Kaplan–Meier method was used to evaluate survival. The 5-year disease-free survival rate of patients with SCLC and LCNEC was lower than that of patients with CLCC (44.4%, 53.0%, and 63.6%, respectively). However, the difference was not statistically significant ($P = 0.1241$; Fig. 5A). Patients with allelic losses at D3S1234 had poorer prognoses than patients without allelic losses. This difference was statistically significant ($P = 0.0481$; Fig. 5B). Patients with allelic losses at D10S1686 had poorer prognoses than patients without

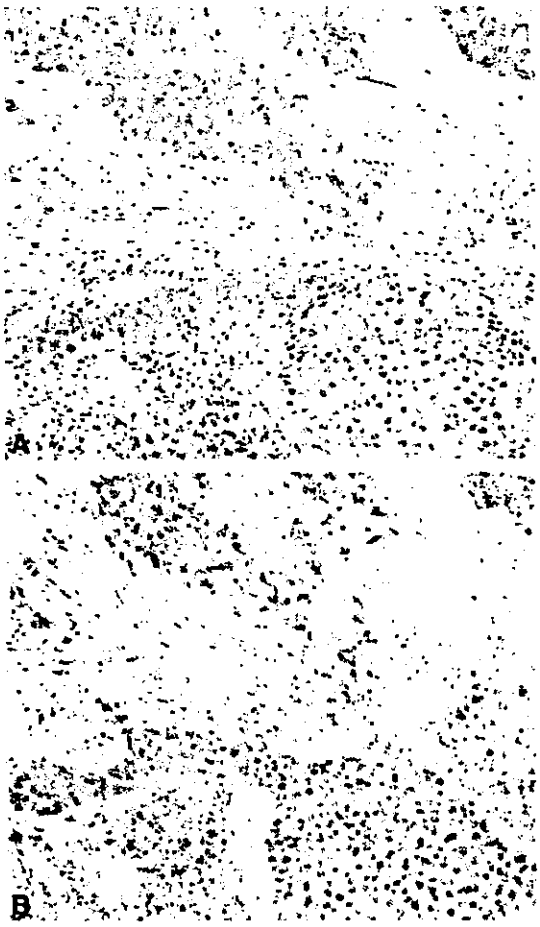

FIGURE 4. Immunohistochemistry for the p16 protein and retinoblastoma (Rb) proteins in combined small cell lung carcinoma (SCLC) with squamous cell carcinoma. (A) Immunohistochemistry using an anti-p16 protein monoclonal antibody (MoAb). The SCLC component stained with the anti-p16 antibody but the squamous cell carcinoma component (right lower) did not stain. (B) Immunohistochemistry using an anti-Rb protein MoAb. The squamous cell carcinoma component (right lower) stained with the anti-Rb MoAb but the SCLC component did not stain.

allelic losses. The difference was statistically significant ($P = 0.0266$; Fig. 5C). Of 22 patients with tumors harboring LOH at D3S1234, 8 underwent postoperative chemotherapy or radiotherapy and 14 did not. Of 14 patients with tumors without LOH at D3S1234, 3 underwent postoperative chemotherapy and 11 did not. There was no significant difference in the frequency of adjuvant therapy between patients with tumors harboring LOH at D3S1234 and those without LOH. Of four patients with tumors harboring LOH at D10S1686, two underwent postoperative chemotherapy and two did not. Of four patients without LOH at D10S1686, one underwent postoperative radiotherapy, and three did not. There was no significant difference in the frequency of adjuvant therapy between patients with tumors harboring LOH at D10S1686 and those without it. Allelic losses at other sites did not appear to influence the survival of the patients studied. The 5-year disease-free survival rate for patients with an FRL ≥ 0.7 was significantly lower than for those with an FRL < 0.7 (43.7% and 61.9%, respectively; $P = 0.0050$). Patients with an FRL ≥ 0.8 had a significantly worse prognosis compared with those with an FRL < 0.8 (39.2% and 62.5%, respectively; $P = 0.0021$; Fig. 5D). Patients with an FRL ≥ 0.9 had a significantly worse prognosis compared with those with an FRL < 0.9 (25.0% and 57.3%, respectively; $P = 0.0123$). The methylation status of the p16 gene did not influence patient survival, nor did immunoreactivity against DO-7, the anti-Rb antibody, and the anti-p16 protein antibody.

DISCUSSION

Distinguishing LCNEC from SCLC can be difficult in some cases. In a study by Travis et al.,[3] there was unanimous diagnostic agreement in 70% of SCLCs and 40% of LCNECs in surgically resected neuroendocrine tumors of the lung that were reviewed independently by five pulmonary pathologists. Most of the disagreements concerned the distinction between SCLC and LCNEC. Marchevsky et al.[4] reported that SCLC and LCNEC demonstrated a continuum of cell size. The distinction between LCNEC and SCLC is important because SCLCs respond initially to chemotherapy but LCNECs do not.

According to Knudson's two-hit theory,[9] loss of function of tumor suppressor genes requires that both alleles be inactivated. One allele is inactivated by allelic loss, whereas the other allele is inactivated by multiple mechanisms including point mutations, aberrant methylation, or other changes that target the individual tumor suppressor gene. Tumor-specific deletions at chromosomal regions suggest the presence of underlying tumor suppressor genes. It is speculated that an accumulation of genetic changes occurs in the development of lung carcinogenesis[10,11] and that the tumor progresses to a more aggressive stage due to accumulation of these defects.[12]

Recently, a genome-wide high-resolution search for LOH was performed on SCLC and NSCLC cell lines.[5,6] These studies showed that some losses are common to both SCLC and NSCLC subtypes, whereas others are subtype specific. It has been suggested that SCLC and NSCLC frequently undergo different genetic

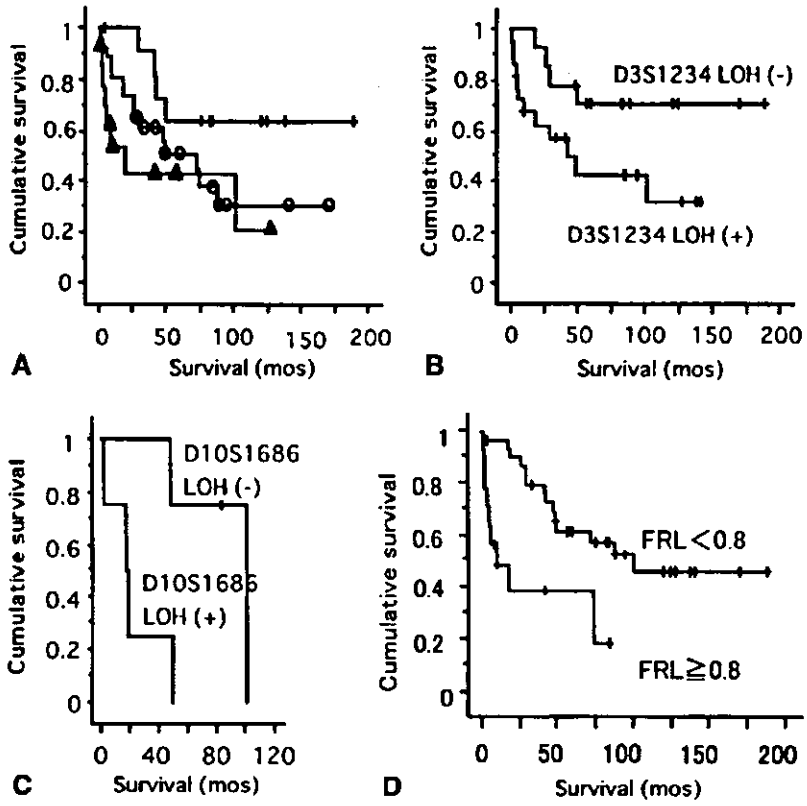

FIGURE 5. (A) Kaplan–Meier survival curves for patients with Stage I classic large cell carcinoma (CLCC), Stage I large cell neuroendocrine carcinoma (LCNEC), and small cell lung carcinoma (SCLC) with limited disease. Five-year survival rates for patients with SCLC and LCNEC were lower than those for patients with CLCC (44.4%, 53.0%, and 63.6%, respectively). However, the difference was not statistically significant. +: CLCC; ○: LCNEC; △: SCLC. (B) Kaplan–Meier survival curves for patients with loss of heterozygosity (LOH) (+) at D3S1234 versus those with no LOH at D3S1234 (-). Patients with LOH at D3S1234 had a worse prognosis than those without LOH at D3S1234 (P = 0.0481). (C) Kaplan–Meier survival curves for patients with LOH at D10S1686 (+) versus those with no LOH at D10S1686 (-). Patients with LOH at D10S1686 had a worse prognosis than those without LOH at D10S1686 (P = 0.0266). (D) Kaplan–Meier survival curves for patients with a high fractional regional loss (FRL) versus those with a low FRL. Patients with an FRL ≥ 0.8 had a significantly worse prognosis compared with those with an FRL < 0.8 (P = 0.0021).

alterations. Onuki et al.[13] evaluated LOH at 3p, 5q, 11q, 13q, 17p and mutations at the p53 and *ras* genes in carcinoid tumors, SCLCs, and LCNECs. They found that the majority of these changes were present in SCLCs and in LCNECs. However, tumor stages were not reported and the authors did not compare these changes with those in CLCCs. Ullmann et al.[14] reported that both SCLC and LCNEC shared several chromosomal aberrations, specifically losses of 3p, 4q, 5q, and 13q and gains of 5p as demonstratd by comparative genome hybridization. However, they suggested that these aberrations could be found in nearly all lung carcinomas. They also showed that a gain of 3p and a loss of 10q and 17p were observed frequently in SCLC but not in LCNEC. Gugger et al.[15] reported that c-myc amplification was observed with a similar frequency in SCLC (20%) and LCNEC (23%).

We evaluated the LOH of Stage I LCNEC and CLCC to elucidate the early genetic changes in neuroendocrine tumors. We then compared the changes with those of SCLC, which is believed to be an aggressive type of lung carcinoma. LOH at TP53 and 13q14 was observed frequently in all subtypes. LOH at 3p14.2, 3p21, and 5q11 was observed more frequently in LCNEC and SCLC than in CLCC. These results suggest that LOH at TP53 and 13q14 is requisite in the development of CLCC, LCNEC, and SCLC, but LOH at 3p and 5q11 is requisite in the development of LCNEC and SCLC. LCNEC is akin to SCLC in terms of loss of alleles at TP53, 13q14, 3p, and 5q11. It is interesting to note that allelic loss at 5q33 was observed frequently in CLCC and in SCLC, but less frequently in LCNEC.

The cyclin-dependent kinase inhibitor, p16, is an important component of cell cycle regulation.[16] The mechanisms by which $p16^{INK4A}$ is inactivated in patients with NSCLCs occur by either homozygous deletions or hypermethylation of the CpG islands or mutations of the $p16^{INK4A}$ gene.[17,18] The immunohistochemical detection of p16 is considered to be a sensitive and reliable method for studying the inactivation of $p16^{INK4A}$ in lung tumors.[19] The results of the current study show that lack of p16 protein expression is observed more frequently in CLCC and in LCNEC than in SCLC. All but one of the SCLC tumor specimens expressed p16 protein. The prevalence of p16

protein expression was not different between CLCC and LCNEC.

p16-negative lung carcinomas expressed Rb protein whereas p16-positive lung carcinomas did not. This was especially evident in specimens of SCLC. None of the p16-positive tumor specimens expressed Rb protein, whereas one p16-negative tumor specimen expressed Rb protein. This finding supports the feedback mechanism of Rb to the level of $p16^{INK4A}$.[20–22] A combined small cell and squamous cell carcinoma specimen showed reciprocal expression of the Rb and p16 proteins. This finding shows that SCLC had developed with the loss of function of Rb and p16 protein expression, whereas squamous cell carcinoma had developed while maintaining the function of the Rb protein.

Aberrant methylation of normally unmethylated CpG islands that are located in or near the promoter region of many genes has been associated with transcriptional inactivation of tumor suppressor genes in human carcinoma. Several genes are frequently methylated in primary lung tumors, including the p16 gene. Aberrant methylation of the p16 gene was detected in precursor lesions of lung carcinomas and is an early event in lung carcinogenesis.[23] Although the frequency of p16 gene methylation is reported to be 25–41% in patients with NSCLC,[24] its frequency is lower in patients with SCLC.[25] We detected methylation of the p16 gene in 33.3% of patients with CLCC and the frequency was comparable to that found in previous reports. The frequency of p16 gene methylation was 47.6% in LCNEC, which was comparable to the rate in CLCC. However, methylation of the p16 gene was not observed in SCLC (0%).

We analyzed pulmonary neuroendocrine carcinomas and found that the prognoses of patients with LCNF, which include LCNEC, LCCNM, and LCCND, are worse than those of patients with CLCC[2] and are comparable to those of patients with SCLC.[26] Onuki et al.[13] reported that LOH at 3p21, the fragile histidine triad (FHIT) gene, 3p22-24, 5q21, 9p21, and the Rb gene correlated with poor survival of patients with neuroendocrine tumors. However, they studied high-grade neuroendocrine and carcinoid tumors together and nearly all of the high-grade neuroendocrine tumors were associated with multiple genetic changes and shorter survivals.

The 3p14.2 region, harbored by the markers D3S1300-D3S1234, is the locus of the FHIT gene. The FHIT gene is frequently abnormal in lung carcinomas. LOH at the FHIT gene locus was observed more frequently in smokers than in nonsmokers, suggesting that FHIT is a molecular target of tobacco smoke carcinogens.[27] A decrease in FHIT protein expression correlated with increased proliferation and larger tumors in patients with breast carcinoma.[28] We examined LOH at 3p14.2 in high-grade neuroendocrine carcinomas and CLCC and found a statistically significant correlation between LOH at 3p14.2 and a poor prognosis ($P = 0.0481$). These results suggest that the FHIT protein may regulate cell proliferation and loss of alleles at the 3p14.2 region may induce the proliferation of tumor cells.

LOH studies have reported a high frequency of deletion at 10q in diverse neoplasms.[29–31] Petersen et al.[31] analyzed lung carcinomas for allelic losses on chromosome 10q. They reported that a high incidence of LOH between 10q21 and 10qter in SCLC and metastatic squamous cell carcinoma was observed and that the presence of LOH correlated significantly with advanced tumor stages. Gasparotto et al.[32] reported a significant association between LOH at 10q and a poor prognosis for patients with head-and-neck squamous cell carcinoma. They suggested that 10q may harbor tumor suppressor gene(s) involved in the progression and aggressiveness of tumors of the upper aerodigestive tract. Although few cases were informative for the evaluation of LOH at D10S1686 in the current study, survival among patients with LOH at D10S1686 was significantly poorer than among patients without LOH. Further analysis of the prognostic importance of LOH at 10q in lung carcinoma will be required.

Allelic losses at TP53 and 13q14 occur in patients with early-stage CLCC, LCNEC, and SCLC. Allelic losses at 3p occur both in LCNEC and SCLC, but not in CLCC. Abnormality of the p16 gene was observed frequently in CLCC and LCNEC, but not in SCLC. Our results show that neuroendocrine differentiation in large cell carcinoma reflects specific genetic changes within the individual neoplasms.

REFERENCES

1. World Health Organization. Histological typing of lung and pleural tumours, 3rd ed. Berlin: Spring-Verlag, 1999:7–12.
2. Iyoda A, Hiroshima K, Toyozaki T, Haga Y, Fujisawa T, Ohwada H. Clinical characterization of pulmonary large cell neuroendocrine carcinoma and large cell carcinoma with neuroendocrine morphology. *Cancer.* 2001;91:1992–2000.
3. Travis WD, Gal AA, Colby TV, Klimstra DS, Falk R, Koss MN. Reproducibility of neuroendocrine lung tumor classification. *Hum Pathol.* 1998;29:272–279.
4. Marchevsky AM, Gal AA, Shah S, Koss MN. Morphometry confirms the presence of considerable nuclear size overlap between "small cells" and "large cells" in high-grade pulmonary neuroendocrine neoplasms. *Am J Clin Pathol.* 2001; 116:466–472.
5. Virmani AK, Fong KM, Kodagoda D, et al. Allelotyping demonstrates common and distinct patterns of chromosomal loss in human lung cancer types. *Genes Chromosomes Cancer.* 1998;21:308–319.

6. Girard L, Zochbauer-Muller S, Virmani AK, Gazdar AF, Minna JD. Genome-wide allelotyping of lung cancer identifies new regions of allelic loss, differences between small cell lung cancer and non-small cell lung cancer, and loci clustering. *Cancer Res.* 2000;60:4894–4906.
7. Herman JG, Graff JR, Myohanen S, Nelkin BD, Baylin SB. Methylation-specific PCR: a novel PCR assay for methylation status of CpG islands. *Proc Natl Acad Sci USA.* 1996; 93:9821–9826.
8. Kaplan EL, Meier P. Nonparametric estimation from incomplete observations. *J Am Stat Assoc.* 1958;53:457–481.
9. Knudson AG Jr. Mutation and cancer: statistical study of retinoblastoma. *Proc Natl Acad Sci USA.* 1971;68:820–823.
10. Hung J, Kishimoto Y, Sugio K, et al. Allele-specific chromosome 3p deletions occur at an early stage in the pathogenesis of lung carcinoma. *JAMA.* 1995;273:558–563.
11. Kishimoto Y, Sugio K, Hung JY, et al. Allele-specific loss in chromosome 9p loci in preneoplastic lesions accompanying non-small-cell lung cancers. *J Natl Cancer Inst.* 1995;87: 1224–1229.
12. Yoshino I, Fukuyama S, Kameyama T, et al. Detection of loss of heterozygosity by high-resolution fluorescent system in non-small cell lung cancer: association of loss of heterozygosity with smoking and tumor progression. *Chest.* 2003; 123:545–550.
13. Onuki N, Wistuba II, Travis WD, et al. Genetic changes in the spectrum of neuroendocrine lung tumors. *Cancer.* 1999;85: 600–607.
14. Ullmann R, Petzmann S, Sharma A, Cagle PT, Popper HH. Chromosomal aberrations in a series of large-cell neuroendocrine carcinomas: unexpected divergence from small-cell carcinoma of the lung. *Hum Pathol.* 2001;32:1059–1063.
15. Gugger M, Burckhardt E, Kappeler A, Hirsiger H, Laissue JA, Mazzucchelli L. Quantitative expansion of structural genomic alterations in the spectrum of neuroendocrine lung carcinomas. *J Pathol.* 2002;196:408–415.
16. Serrano M, Hannon GJ, Beach D. A new regulatory motif in cell-cycle control causing specific inhibition of cyclin D/CDK4. *Nature.* 1993;366:704–707.
20. Li Y, Nichols MA, Shay JW, Xiong Y. Transcriptional repression of the D-type cyclin-dependent kinase inhibitor p16 by the retinoblastoma susceptibility gene product pRb. *Cancer Res.* 1994;54:6078–6082.
17. Cairns P, Polascik TJ, Eby Y, et al. Frequency of homozygous deletion at p16/CDKN2 in primary human tumours. *Nat Genet.* 1995;11:210–212.
18. Merlo A, Herman JG, Mao L, et al. 5′ CpG island methylation is associated with transcriptional silencing of the tumour suppressor p16/CDKN2/MTS1 in human cancers. *Nat Med.* 1995;1:686–692.
19. Gazzeri S, Gouyer V, Vour'ch C, Brambilla C, Brambilla E. Mechanisms of p16INK4A inactivation in non small-cell lung cancers. *Oncogene.* 1998;16:497–504.
21. Otterson GA, Kratzke RA, Coxon A, Kim YW, Kaye FJ. Absence of p16INK4 protein is restricted to the subset of lung cancer lines that retains wildtype RB. *Oncogene.* 1994;9: 3375–3378.
22. Shapiro GI, Edwards CD, Kobzik L, et al. Reciprocal Rb inactivation and p16INK4 expression in primary lung cancers and cell lines. *Cancer Res.* 1995;55:505–509.
23. Belinsky SA, Nikula KJ, Palmisano WA, et al. Aberrant methylation of p16(INK4a) is an early event in lung cancer and a potential biomarker for early diagnosis. *Proc Natl Acad Sci USA.* 1998;95:11891–11896.
24. Zochbauer-Muller S, Gazdar AF, Minna JD. Molecular pathogenesis of lung cancer. *Annu Rev Physiol.* 2002;64:681–708.
25. Toyooka S, Toyooka KO, Maruyama R, et al. DNA methylation profiles of lung tumors. *Mol Cancer Ther.* 2001;1:61–67.
26. Iyoda A, Hiroshima K, Baba M, Saitoh Y, Ohwada H, Fujisawa T. Pulmonary large cell carcinomas with neuroendocrine features are high-grade neuroendocrine tumors. *Ann Thorac Surg.* 2002;73:1049–1054.
27. Sozzi G, Sard L, De Gregorio L, et al. Association between cigarette smoking and FHIT gene alterations in lung cancer. *Cancer Res.* 1997;57:2121–2123.
28. Campiglio M, Pekarsky Y, Menard S, Tagliabue E, Pilotti S, Croce CM. FHIT loss of function in human primary breast cancer correlates with advanced stage of the disease. *Cancer Res.* 1999;59:3866–3869.
29. Herbst RA, Weiss J, Ehnis A, Cavenee WK, Arden KC. Loss of heterozygosity for 10q22-10qter in malignant melanoma progression. *Cancer Res.* 1994;54:3111–3114.
30. Gray IC, Phillips SM, Lee SJ, Neoptolemos JP, Weissenbach J, Spurr NK. Loss of the chromosomal region 10q23-25 in prostate cancer. *Cancer Res.* 1995;55:4800–4803.
31. Petersen S, Wolf G, Bockmuhl U, Gellert K, Dietel M, Petersen I. Allelic loss on chromosome 10q in human lung cancer: association with tumour progression and metastatic phenotype. *Br J Cancer.* 1998;77:270–276.
32. Gasparotto D, Vukosavljevic T, Piccinin S, et al. Loss of heterozygosity at 10q in tumors of the upper respiratory tract is associated with poor prognosis. *Int J Cancer.* 1999; 84:432–436.

Available online at www.sciencedirect.com
SCIENCE DIRECT®
Immunology Letters 92 (2004) 143–147
Immunology Letters
www.elsevier.com/locate/

Cysteine-dependent immune regulation by TRX and MIF/GIF family proteins

Norihiko Kondo[a,b], Yasuyuki Ishii[b], Aoi Son[a], Junko Sakakura-Nishiyama[c], Yong-Won Kwon[b], Masaki Tanito[a], Yumiko Nishinaka[b], Yoshiyuki Matsuo[b], Toshinori Nakayama[d], Masaru Taniguchi[e,f], Junji Yodoi[a,b,*]

[a] *Department of Biological Responses, Institute of Virus Research, Kyoto University, 53 Kawaharacho, Shogoin, Sakyo-ku, Kyoto 606-8507, Japan*
[b] *BioMedical Special Research Unit, Human Stress Signal Research Center, National Institute of Advanced Industrial Science and Technology (AIST), Midorigaoka, Ikeda, Osaka 563-8577, Japan*
[c] *Redox Bio Science Inc., 82-1 Shimotsutsumi-cho, Kawabata, Marutamachi, Sakyo-ku, Kyoto 606-8396, Japan*
[d] *Department of Medical Immunology and Department of Molecular Immunology, Graduate School of Medicine, Chiba University, 1-8-1 Inohana, Chuo-ku, Chiba 260-8670, Japan*
[e] *Department of Molecular Immunology, Graduate School of Medicine, Chiba University, 1-8-1 Inohana, Chuo-ku, Chiba 260-8670, Japan*
[f] *Laboratory for Immune Regulation, RIKEN Research Center for Allergy and Immunology, Yokohama 230-0045, Japan*

Received 20 October 2003; accepted 25 November 2003

Abstract

Thioredoxin (TRX) superfamily proteins that contain a conserved redox-active site -Cys-Xa.a.-Xa.a.-Cys- includes proinflammatory cytokine, macrophage migration inhibiting factor (MIF) and the immune regulatory cytokine, glycosylation inhibiting factor (GIF) in which Cys-60 is cysteinylated. In this report, we have analyzed the functional interaction between TRX and MIF/GIF. The stable Jurkat T cell line transfected with human TRX gene (TRX-transfectant) was highly resistant to hydrogen peroxide-induced apoptosis, but not the cell line transfected with vector (mock-transfectant). The expression level of MIF/GIF protein of TRX-transfectant was lower than that of mock-transfectant. Conversely, the expression level of intracellular TRX protein in $CD4^+$-T cells derived from MIF −/− mice were significantly higher than that from background BALB/c mice. These findings collectively suggest that oxidative stress-induced apoptosis on T lymphocytes might be protected by the reciprocal regulation of TRX and MIF/GIF expression.
© 2004 Elsevier B.V. All rights reserved.

Keywords: Thioredoxin (TRX); Redox; GIF/MIF

1. Introduction

Thioredoxin (TRX) is a 12 kDa protein with redox-active dithiol in the conserved active site; -Cys^{32}-Gly-Pro-Cys^{35}- [1]. Human TRX was originally cloned as a soluble factor named adult T-cell leukemia-derived factor (ADF) produced by human T cell leukemia virus type-I transformed ATL2 cells [2]. TRX superfamily in mammalian possessing the redox-active site; -Cys-Xa.a.-Xa.a.-Cys- is composed of 17 proteins; TRX, TRX-2 [3], spTRX [4], TMX [5] or etc. TRX is induced by a variety of oxidative stresses including viral infection and anti-cancer agents. It was recently reported that antigen-presenting cells secrete TRX for the activation of T lymphocytes [6]. Although the releasing mechanism is still unclear, the secretion of TRX is associated with the cellular resistance to cisplatin- or ethanol-induced oxidative stress [7,8]. Intracellular TRX plays crucial roles in the scavenging of reactive oxygen species with peroxiredoxin, the regulation of redox-sensitive transcription factors including AP-1 and NF-κB or the negative regulator of apoptosis signal-regulating kinase (ASK) 1, suggesting that TRX functions for redox regulation of the apoptosis signal transduction pathway as well as the effects of antioxidants against cytokine- and stress-induced apoptosis [9]. As other TRX family proteins for regulation of apoptosis, proinflammatory cytokines or immune re-

* Corresponding author. Tel.: +81-75-751-4024; fax: +81-75-761-5766.
E-mail address: yodoi@virus.kyoto-u.ac.jp (J. Yodoi).

0165-2478/$ – see front matter © 2004 Elsevier B.V. All rights reserved.
doi:10.1016/j.imlet.2003.11.030

sponse, macrophage migration inhibiting factor (MIF) and glycosylation inhibitory factor (GIF) are addressed [10]. Although MIF and GIF share an identical structure gene, the generation of immunosuppressive activity of GIF is required for cysteinylation at Cys^{60} in the redox-active site; -Cys^{57}-Ala-Leu-Cys^{60} [11]. MIF is a pivotal mediator of innate immunity and sustains macrophage proinflammatory function by inhibiting p53 [12,13]. It is recently reported that MIF is a modulator of pro-oxidative stress-induced apoptosis of HL-60 [14]. An interest has herein arisen how TRX and MIF/GIF regulate oxidative stress-induced apoptosis of T lymphocytes. We reveal that both oxidative stress and overexpression of intracellular TRX suppress MIF expression in T cell line and TRX expression is accelerated in $CD4^+$ T cells derived from MIF-deficient mice.

2. Materials and methods

2.1. Reagents and cells

Jurkat (human T lymphocyte cell line) cells were cultured in RPMI 1640 medium supplemented with 10% heat-inactivated fetal calf serum, 100 units/ml penicillin, and 100 μg/ml streptomycin in 5% CO_2 at 37 °C. $CD4^+$ T cells were purified from spleens of MIF −/− mice [15] by using magnetic beads (Miltenyi Biotec, Bergisch Gladbach, Germany).

2.2. Plasmid DNA

The DNA fragments for encoding TRX gene were amplified by PCR method using the pcDNA3.1 encoding human TRX cDNA as template [2] and were inserted to p3xFLAG-CMV-10 vector (Sigma–Aldrich).

2.3. Stable transfectants for TRXs

For stable expression of the TRX gene and protein, Jurkat T cell line was transfected with 10 μg of TRX-cDNA/p3XFLAG-CMV-10 plasmid DNA by using electroporation on the condition of a single brief electronic pulse of 800 V/cm and duration of 20–24 ms at room temperature (Gene PulserII, Bio-Rad). The transfectants were cultured in RPMI1640 containing 400 μg/ml of neomycin (G418) (Nacalai tesque) to screen stable transfectants. The drug-resistant bulk population of the cells was cloned by limiting dilution. Expression of TRX protein on the cells was confirmed by Western blot analysis. To avoid variation among clones, three randomly selected clones were tested.

2.4. Assay for apoptosis

After the cells were stimulated with H_2O_2 for 24 h, the cell lysate was prepared with lysis buffer including the 1% Nonidet P-40 in 50 mM Tris–HCl (pH7.5) for the measurement of caspase-3 activity whereas the cells were treated with 50 μg/ml propidium iodide (Calbiochem) for the measurement of sub-G1 DNA content by flow cytometer (FACSCalibur, Becton Dickinson) using CELLQUEST software, respectively [16]. The caspase 3 activity in this lysate was measured by a fluorometer (Spectra Fluor, Tecan) as previous described [17].

2.5. SDS–PAGE and Western blot analysis

SDS–PAGE was performed through 4% stacking and 15% separating gels by electrophoresis system (Mini Protean III Cell, Bio-Rad). For Western blotting, the proteins separated by SDS–PAGE gel were transferred to a polyvinylidene difluoride (PVDF) membrane (Immobilon-P, Millipore) using a semi-dry electrophoresis transfer apparatus (Trans-Blot SD Semi-dry Transfer Cell, Bio-Rad). Membranes were blocked with phosphate buffer saline (PBS) containing 0.05% (v/v) Tween 20 (PBS-t) including 5% skim milk (blocking buffer) for 1 h at 4 °C. For the detection of FLAG-tagged proteins, the membrane was incubated with blocking buffer including horseradish peroxidase-conjugated anti-FLAG Ig (FLAG M2, Sigma–Aldrich) for 1 h. For the detection of MIF/GIF protein, the membrane was incubated with blocking buffer including rabbit anti-GIF polyclonal antibodies [11] for 2 h, followed by horseradish peroxidase-conjugated anti-rabbit Ig (Amersham Biosciences) for 1 h. After washing with excess PBS-t buffer, the protein band was detected by ECL or ECL Plus Western blotting detection system (Amersham Biosciences).

3. Results

3.1. Hydrogen peroxide-induced apoptosis is inhibited by overexpression of intracellular TRX

In this report, we tried to elucidate the cross-talk among TRX superfamily proteins in oxidative stress-induced apoptosis of T cells. To assess the functions of TRX superfamily proteins, Jurkat T cells transfected with human TRX-wild-type gene (TRX-transfectant) or control vector (mock-transfectant) was prepared, respectively. As a preliminary experiment to test whether hydrogen peroxide (H_2O_2) induces apoptosis of TRX-tranfectant or mock-transfectant, both caspase-3 activity and sub G1 population in the tranfectants were measured at 24 h after the addition of 50 μM H_2O_2 in the culture. As shown in Fig. 1A, the caspase-3 activity of the TRX-transfectant was significantly lower than mock-transfectant. The apoptosis rate was determined as % DNA content of sub G1 by flow cytometric analysis using PI staining (Fig. 1B). Without the addition of H_2O_2, the DNA contents of sub G1 were 3.3% in mock-transfectant or 3.6% in TRX-transfectant. The mock- or TRX-tranfectant showed 15.5 or 9.4% apoptosis at 48 h after the addition of H_2O_2, respectively. These results indicate that the Jurkat T

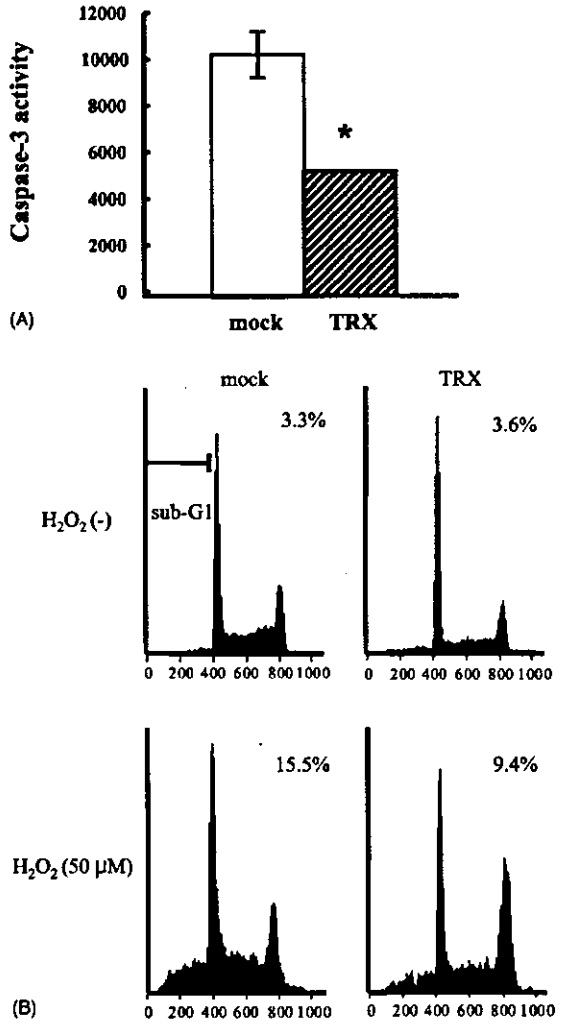

Fig. 1. Protection of stable transfectants overexpressing TRX against oxidative stress. (A) Caspase-3 activities of transfectants were measured 24 h after the stimulation with 50 μM H_2O_2. $^*P < 0.01$; when compared with control. (B) The Jurkat transfectant cells were cultured in the presence of 50 μM of H_2O_2 for 48 h. Then the cells were fixed by 70% ethanol on ice overnight. After washing the several times with exceed PBS(−) buffer, the cells were treated with 50 μg/ml of RNase for 1 h at 37 °C. After incubation with PI staining solution for 1 h, the cells were analyzed by flowcytometer.

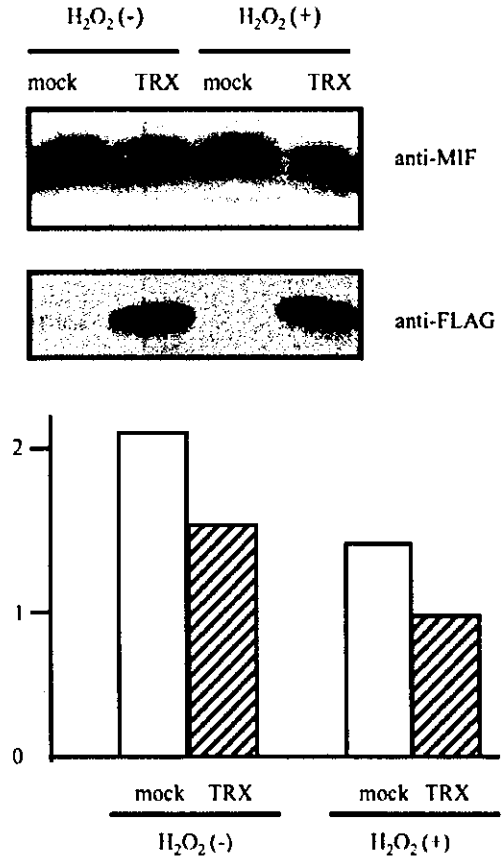

Fig. 2. Suppression of MIF expression in Jurkat T cell line by overexpression of TRX. Jurkat transfectant cells of vector (mock) or human TRX cDNA gene were cultured in the absence or presence of 50 μM H_2O_2 for 24 h and lysed with lysis buffer containing 1% NP-40. Each cell lysate was analyzed by SDS–PAGE, followed by Western blotting using anti-MIF/GIF polyclonal antibodies. Bottom panel: densitometric analysis of MIF/GIF expression. Normalized with total weight of applied proteins. 200 μg.

cell transfectant expressing a large amount of intracellular TRX is protective to H_2O_2-induced apoptosis.

3.2. Expression level of MIF/GIF is suppressed by overexpression of intracellular TRX and hydrogen peroxide

To elucidate the mechanism of anti-apoptotic effect by overexpression of TRX, the involvement of MIF/GIF protein among TRX superfamily was analyzed. Expression level of endogenous MIF/GIF in mock- or TRX-transfectant was determined by Western blotting using anti-MIF/GIF polyclonal antibodies in the absence or presence of H_2O_2. As shown in Fig. 2, the expression level of MIF/GIF protein of the TRX-transfectant was lower than that of the mock-transfectant despite the existence of H_2O_2. Moreover, the production of MIF/GIF protein in both mock- and TRX-transfectant was suppressed in the presence of H_2O_2. The data indicate that MIF/GIF expression is negatively regulated by the intracellular TRX and H_2O_2.

3.3. TRX expression is suppressed in T lymphocytes derived from MIF/GIF −/− mice

In order to clarify the cross-talk between TRX and MIF/GIF, the expression level of intracellular TRX protein was examined on T lymphocytes derived from MIF/GIF−/−

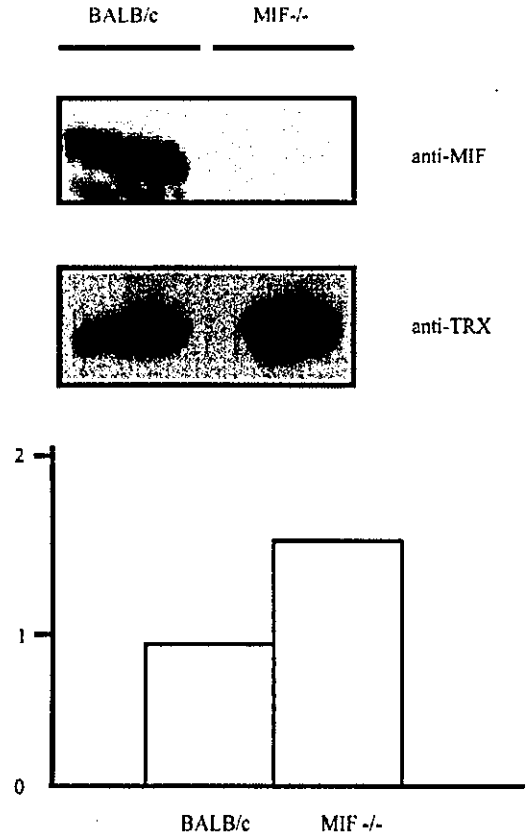

Fig. 3. Suppression of TRX expression in naïve T cells derived from MIF/GIF−/− mice. $CD4^+$ T cells were purified from spleens of MIF−/− or BALB/c mice and lysed with lysis buffer containing 1% NP-40. Each cell lysate was analyzed by SDS–PAGE, followed by Western blotting using anti-MIF/GIF polyclonal antibodies or anti-TRX mAb. Bottom panel: densitometric analysis of TRX expression. Normalized with total weight of applied proteins, 50 μg.

mice. $CD4^+$ T cells in spleens derived from MIF/GIF−/− mice or background BALB/c mice were enriched by depletion of negative lineage populations, respectively. The cells were cultured 24 h, and lysed with the solution containing 1% Nonidet P-40. Then, the samples were analyzed by SDS–PAGE and Western blotting using anti-MIF/GIF or anti-TRX mAb, respectively. Fig. 3 clearly showed that endogenous TRX expression in $CD4^+$ T cells derived from MIF/GIF−/− mice was augmented than that from BALB/c mice.

4. Discussion

In the present study, we have shown that the expression level of both TRX and MIF/GIF in TRX superfamily is regulated each other in the course of oxidative stress-induced apoptosis on T lymphocytes. We have already reported that human TRX has been shown to be a scavenger of reactive oxygen species (ROS), and recombinant human TRX performs a protective activity against hydrogen peroxide-induced cytotoxicity [18]. In fact, overexpression of human TRX in Jurkat T cell-transfectant resulted in the protection against H_2O_2-induced apoptosis (Fig. 1). This phenomenon might be in part interpreted as the scavenging activity of ROS and the inhibition of ASK1 kinase activity by intracellular TRX. However, the effects of other TRX family proteins have remained to be solved.

In a recent report, MIF has been addressed as a member of the thioredoxin family [10]. Although MIF was firstly identified as a soluble T cell-derived inhibitory factor for macrophage migration, the product of gene cloned was ubiquitously expressed in a variety of cells [19]. Despite GIF which shares an identical structure gene with MIF, is a suppressor T (Ts) cell-derived immunosuppressive cytokine and a derivative by the post-translational cysteinylation at Cys-60, the intracellular product in Ts cells is the unmodified form, MIF [11]. In the most recent report, a 16 residues peptide fragment of MIF (50–65) containing Cys^{57}-Ala-Leu-Cys^{60} exhibits redox activity, and had MIF-like biological functions [20]. Taken together the above evidences, it is suggested that the modification of MIF/GIF protein secreted from cells may be regulated by redox state. In contrast, it had yet remained to be solved whether homogenous MIF in cells interacts with other TRX family proteins or is regulated by redox state. Fig. 2 showed that the expression of MIF protein was suppressed by the overexpression of TRX or the presence of H_2O_2. In the recent reports, MIF inhibits p53 tumor suppressor activity in macrophage cell lines [12,14]. If MIF functions as a negative regulator of p53 in T lymphocytes, one may expect that the inhibition of MIF expression results in the enhancement of oxidative stress-induced apoptosis. In the mock-transfectant, the enhancement of apoptosis by H_2O_2 was correlated with the downregulation of MIF expression (Figs. 1 and 2). However, MIF expression in the TRX-transfectant was less than that in mock in the presence or absence of H_2O_2 (Fig. 2). We address two interpretations of this paradox. One is that TRX may function as a negative regulator of p53 and share some functions with MIF. The other is that overexpression of TRX may compensate via other regulatory pathways of oxidative stress-induced apoptosis for the downregulation of MIF expression accompanying the loss of p53 inactivation as one anti-apoptotic activity. In our previous report, TRX augmented the DNA binding activity of p53, indicating coupling of the oxidaitive stress response and p53-dependent repair mechanism by TRX dependent redox regulation [21]. Although the cooperative regulation of apoptosis by TRX and MIF is still obscure, it is likely that the intracellular TRX and MIF regulate each other expression. Actually, the expression level of TRX protein in $CD4^+$ T cells derived from MIF−/− mice was obviously higher than that from background BALB/c mice (Fig. 3). This result suggests that TRX ex-

pression might be negatively regulated by MIF. Roger et al. have reported that MIF-deficient macrophages are hyporesponsive to lipopolysaccharide (LPS) and Gram-negative bacteria, as shown by a profound reduction in the activity of NF-κB, the production of tumor-necrosis factor-alpha and the expression of Toll-like receptor 4 (TLR4) [22]. In our unpublished data, $CD11c^+$ DC derived from spleens of TRX-transgenic mice produces less amount of IL-12 than that from B6 background. These data collectively indicate that intracellular ratio of TRX and MIF proteins may regulate TLR4-mediated signal transduction.

Acknowledgements

We thank H. Nakamura, H. Masutani, Y.C. Kim and A. Teratani for excellent technical assistance and discussion, and both Y. Kanekiyo and Maina Ueshima for secretarial help.

References

[1] Holmgren A. Annu Rev Biochem 1985;54:237–71.
[2] Tagaya Y, Maeda Y, Mitsui A, Kondo N, Matsui H, Hamuro J, et al. EMBO J 1989;8:757–64.
[3] Pedrajas JR, Kosmidou E, Miranda-Vizuete A, Gustafsson JA, Wright AP, Spyrou G. J Biol Chem 1999;274:6366–73.
[4] Miranda-Vizuete A, Ljung J, Damdimopoulos AE, Gustafsson JA, Oko R, Pelto-Huikko M, et al. J Biol Chem 2001;276:31567–74.
[5] Matsuo Y, Akiyama N, Nakamura H, Yodoi J, Noda M, Kizaka-Kondoh S. J Biol Chem 2001;276:10032–8.
[6] Angelini G, Gardella S, Ardy M, Ciriolo MR, Filomeni G, Di Trapani G, et al. Proc Natl Acad Sci USA 2002;99:1491–6.
[7] Sasada T, Nakamura H, Ueda S, Iwata S, Ueno M, Takabayashi A, et al. Antioxid Redox Signal 2000;2:695–705.
[8] Hirota K, Nakamura H, Arai T, Ishii H, Bai J, Itoh T, et al. Biochem Biophys Res Commun 2000;275:825–30.
[9] Saitoh M, Nishitoh H, Fujii M, Takeda K, Tobiume K, Sawada Y, et al. EMBO J 1998;17:2596–606.
[10] Potolicchio I, Santambrogio L, Strominger JL. J Biol Chem 2003;278:30889–95.
[11] Watarai H, Nozawa R, Tokunaga A, Yuyama N, Tomas M, Hinohara A, et al. Proc Natl Acad Sci USA 2000;97:13251–6.
[12] Hudson JD, Shoaibi MA, Maestro R, Carnero A, Hannon GJ, Beach DH. J Exp Med 1999;190:1375–82.
[13] Mitchell RA, Liao H, Chesney J, Fingerle-Rowson G, Baugh J, David J, et al. Proc Natl Acad Sci USA 2002;99:345–50.
[14] Nguyen MT, Lue H, Kleemann R, Thiele M, Tolle G, Finkelmeier D, et al. J Immunol 2003;170:3337–47.
[15] Honma N, Koseki H, Akasaka T, Nakayama T, Taniguchi M, Serizawa I, et al. Immunology 2000;100:84–90.
[16] Kwon YW, Ueda S, Ueno M, Yodoi J, Masutani H. J Biol Chem 2002;277:1837–44.
[17] Bai J, Nakamura H, Hattori I, Tanito M, Yodoi J. Neurosci Lett 2002;321:81–4.
[18] Nakamura H, Matsuda M, Furuke K, Kitaoka Y, Iwata S, Toda K, et al. Immunol Lett 1994;42:75–80.
[19] Weiser WY, Temple PA, Witek-Giannotti JS, Remold HG, Clark SC, David JR. Proc Natl Acad Sci USA 1989;86:7522–6.
[20] Nguyen MT, Beck J, Lue H, Funfzig H, Kleemann R, Koolwijk P, et al. J Biol Chem 2003;278:33654–71.
[21] Ueno M, Masutani H, Arai RJ, Yamauchi A, Hirota K, Sakai T, et al. J Biol Chem 1999;274:35809–15.
[22] Roger T, David J, Glauser MP, Calandra T. Nature 2001;414:920–4.

THE JOURNAL OF BIOLOGICAL CHEMISTRY
Vol. 279, No. 22, Issue of May 28, pp. 23123–23133, 2004
Printed in U.S.A.
© 2004 by The American Society for Biochemistry and Molecular Biology, Inc.

CD28 Costimulation Controls Histone Hyperacetylation of the Interleukin 5 Gene Locus in Developing Th2 Cells*

Received for publication, February 4, 2004, and in revised form, March 22, 2004
Published, JBC Papers in Press, March 23, 2004, DOI 10.1074/jbc.M401248200

Masamichi Inami‡, Masakatsu Yamashita‡, Yoshiyuki Tenda‡, Akihiro Hasegawa‡, Motoko Kimura‡, Kahoko Hashimoto§, Nobuo Seki¶, Masaru Taniguchi‖, and Toshinori Nakayama‡**

From the ‡Department of Immunology, Graduate School of Medicine, Chiba University, 1-8-1 Inohana Chuo-ku, Chiba 260-8670, §Department of Life and Environmental Sciences and High Technology Research Center, Chiba Institute of Technology, Narashino, Tsudanuma, Chiba 275-0016, ¶Exploratory Research Laboratories, Department of Bioscience, Fujisawa Pharmaceutical Co. Ltd., 5-2-3, Tokodai, Tsukuba, Ibaraki 300-2698, and ‖Laboratory for Immune Regulation, RIKEN Research Center for Allergy and Immunology, Yokohama 230-0045, Japan

Interleukin 5 (IL-5) plays a unique role in allergic inflammatory responses, and the understanding of molecular mechanisms underlying the generation of IL-5-producing cells is crucial for the regulation of allergic disorders. Differentiation of naive CD4 T cells into type-2 helper (Th2) cells is accompanied by chromatin remodeling including hyperacetylation of histones H3 and H4 in the nucleosomes associated with the IL-4, IL-13, and IL-5 genes. Histone hyperacetylation of the IL-5 gene displayed a delayed kinetics compared with that of the IL-4 and IL-13 genes, suggesting a distinct remodeling mechanism for the IL-5-gene locus. Here we studied the role of CD28 costimulation in the generation of IL-5-producing cells and the histone hyperacetylation of the IL-5 gene locus. CD28-costimulation selectively enhanced histone hyperacetylation of the IL-5 gene locus that appeared to be mediated through NF-κB activation and subsequent up-regulation of GATA3. The CD28 costimulation-sensitive histone hyperacetylation spanned almost the entire intergenic region between the IL-5 and RAD50 accompanied with intergenic transcript. Thus, this is the first demonstration that CD28 costimulation controls a chromatin-remodeling process during Th2 cell differentiation.

Upon antigen recognition by T cell receptor (TCR),[1] naive CD4 T cells differentiate into two distinct helper T (Th) cell subsets, Th1 and Th2 cells (1). Th1 cells produce IFNγ and tumor necrosis factor-β and initiate cell-mediated immunity against intracellular pathogens. Th2 cells produce IL-4, IL-5, and IL-13 and are involved in humoral immunity and allergic responses. The cytokine environment is crucial in controlling the direction of Th cell differentiation (2, 3). For Th1 cell differentiation, IL-12-mediated activation of signal transducer and activator of transcription (STAT) 4 is required, whereas IL-4-mediated STAT6 activation is important for Th2 cell generation (4–6). In addition, TCR stimulation events upon encounter with antigens are also indispensable for both Th1 and Th2 cell differentiation. We reported that efficient TCR-mediated activation of the $p56^{lck}$, calcineurin, and Ras-extracellular signal-regulated kinase mitogen-activated protein kinase signaling cascade is crucial for Th2 cell differentiation (7–9). Recent studies have identified several transcription factors that control Th1/Th2 cell differentiation (10). Among them, GATA3 appears to be a master transcription factor for Th2 cell differentiation. GATA3 is selectively induced in developing Th2 cells, and the ectopic expression of GATA3 induced Th2 cell differentiation even in the absence of IL-4 or STAT6 (11–14). For Th1 cell differentiation, T-bet was recently identified as a key transcription factor (15).

CD28 costimulation enhances Th2 responses significantly (16, 17). Upon anti-CD28 mAb stimulation, phosphatidylinositol 3-kinase is recruited to CD28 and activated, and then subsequent activation of NF-κB is induced (18–21). It has been reported that GATA3 induction was an outcome of the CD28-induced NF-κB activation in T cells (22, 23). This may be a mechanism by which Th2 responses were enhanced by CD28 costimulation. It is also known that IL-5 production and IL-5-dependent airway inflammation are dependent on NF-κB family members (24–26).

Chromatin remodeling of the Th2 cytokine gene loci (IL-4/IL-5/IL-13) occurs during Th2 cell differentiation (27). A highly conserved 400-bp noncoding sequence 1 (CNS1) was identified, and an important role in coordinate expression of Th2 cytokines was revealed (28, 29). More recently, a 3′ distal IL-4 enhancer (V_A) containing an inducible DNase I hypersensitive site was identified (30). Reiner and co-workers (31) report that demethylation of the intron 2 region of the IL-4 gene was associated with cell cycle progression and Th2 cell differentiation (31). We reported that demethylation of this region is regulated by *polycomb* group genes (32) that are known to

* This work was supported by grants from the Ministry of Education, Culture, Sports, Science, and Technology of (Japan) (Grants-in-aid for Scientific Research, Priority Areas Research 13218016 and 12051203 and Scientific Research B 14370107, Advanced and Innovational Research Program in Life Science, and Special Coordination Funds), the Ministry of Health, Labor, and Welfare (Japan) (a grant-in-aid for research on Advanced Medical Technology), the Program for Promotion of Fundamental Studies in Health Science of the Organization for Pharmaceutical Safety and Research (Japan), Human Frontier Science Program Research Grant RG00168/2000-M206, the Hamaguchi Foundation, and the Uehara Memorial Foundation. The costs of publication of this article were defrayed in part by the payment of page charges. This article must therefore be hereby marked "*advertisement*" in accordance with 18 U.S.C. Section 1734 solely to indicate this fact.

** To whom correspondence should be addressed: Dept. of Immunology, Graduate School of Medicine, Chiba University, 1-8-1 Inohana Chuo-ku, Chiba 260-8670, Japan. Tel.: 81-43-226-2200; Fax: 81-43-227-1498; E-mail: tnakayama@faculty.chiba-u.jp.

[1] The abbreviations used are: TCR, T cell receptor; Th cells, helper T cells; IFN, interferon; STAT, signal transducers and activators of transcription; IL, interleukin; mAb, monoclonal antibody; ELISA, enzyme-linked immunosorbent assay; CNS1, conserved noncoding sequence 1; ChIP, chromatin immunoprecipitation; GFP, green fluorescent protein; EGFP, enhanced GFP; RT, reverse transcription; IRES, internal ribosome entry site; CREB, cAMP-response element-binding protein.

regulate transcriptional memory in *Drosophila*.

Hyperacetylation of histone H3 and H4 by histone acetyltransferases was suggested to be associated with active chromatin (33). Recently, we and others have demonstrated that histone hyperacetylation of the Th2 cytokine gene loci occurs in developing Th2 cells in a Th2-specific and STAT6-dependent manner (34–36). We demonstrated an essential role for GATA3 in the Th2-specific hyperacetylation (34). We also generated a precise map of the Th2-specific histone hyperacetylation within the IL-13 and IL-4 gene loci and identified a 71-bp conserved GATA3 response element 1.6 kilobase pairs upstream of IL-13 locus exon 1. This histone hyperacetylation remodeling process could be a major target for the Th2 master transcription factor GATA3 to induce differentiation toward Th2 cells.

Histone hyperacetylation of another Th2 cytokine gene locus, IL-5, occurs in a Th2-specific STAT6- and GATA3-dependent manner with significantly different kinetics compared with that of the IL-4 and IL-13 genes (34). The direction of transcription of the IL-5 gene is opposite to that of IL-13 and IL-4. In addition, the RAD50 gene encoding a DNA repair enzyme is located between the IL-5 and IL-13 gene loci. A differential role for GATA3 in the regulation of promoter activity of the IL-5 gene from IL-4 has been suggested (37–39). These results encouraged us to explore possible novel molecular mechanisms that would govern histone hyperacetylation of the IL-5 gene locus.

In the present study we investigated histone hyperacetylation of the IL-5 gene locus in developing Th2 cells cultured with or without CD28 costimulation. A long range CD28-sensitive Th2-specific histone hyperacetylation was detected in the IL-5 and intergenic region of the IL-5 and RAD50 gene loci. The hyperacetylation was accompanied by CD28-sensitive intergenic transcripts and required high expression of GATA3. A molecular mechanism that governs Th2-specific histone hyperacetylation of the IL-5-gene associated nucleosomes will be discussed.

MATERIALS AND METHODS

Mice—C57BL/6 mice were purchased from SLC (Shizuoka, Japan). STAT6-deficient (KO) mice were kindly provided by Shizuo Akira (Osaka University, Osaka, Japan) (40). All mice used in this study were maintained under specific-pathogen-free conditions and were about 4 weeks old. Animal care was in accordance with the guidelines of Chiba University.

Immunofluorescent Staining and Flow Cytometry Analysis—In general, one million cells were stained with appropriate specific antibodies according to a standard method (41, 42). For intracellular staining, fluorescein isothiocyanate-conjugated anti-IFN-γ antibody (XMG1.2; Pharmingen), phosphatidylethanolamine-conjugated anti-IL-4 antibody (11B11; Pharmingen), and allophycocyanin-conjugated anti-IL-5 antibody (TRFK5; Pharmingen) were used. To detect intracellular IL-13, biotinylated polyclonal anti-IL-13 antibody (R&D Systems), and phosphatidylethanolamine-conjugated avidin were used. Flow cytometry analysis was performed on a FACScalibur (BD Biosciences), and results were analyzed by CELLQUEST software (BD Biosciences).

Cell Cultures and in Vitro T Cell Differentiation—Splenic CD4 T cells were stained with anti-CD4-fluorescein isothiocyanate and then purified using magnetic beads and an Auto-MACS sorter® (Miltenyi Biotec), yielding a purity of >98%. Enriched CD4 T cells (1.5×10^6) were stimulated for 2 days with immobilized anti-TCR mAb (H57-597, 3 μg/ml) and soluble anti-CD28 mAb (37.51, 3 μg/ml) in the presence of IL-2 (25 units/ml), IL-12 (100 units/ml), and anti-IL-4 mAb (11B11, 25% culture supernatant) for Th1-skewed conditions. For Th2-skewed conditions, cells were stimulated with immobilized anti-TCR mAb as above but in the presence of IL-2 (25 units/ml), IL-4 (100 units/ml), and anti-IFNγ mAb (R4.6A2, 25% culture supernatant). The cells were then transferred to new dishes and cultured for another 5 days in the presence of immobilized anti-TCR mAb, soluble anti-CD28 mAb, and the cytokines present in the initial culture. To enhance the generation of IL-5-producing cells, stimulation with anti-TCR and anti-CD28 mAbs was performed during the second culture for 5 days. This procedure is slightly different from that used in our previous report (16). Where indicated, wortmannin (Calbiochem) was added to the culture at the doses of 30 or 300 nM for the first 2 days. *In vitro* differentiation was then assessed by intracellular cytokine staining with anti-IL-4, anti-IL-5, anti-IL-13, and anti-IFNγ or by ELISA as described (42).

Chromatin Immunoprecipitation (ChIP) Assay—The ChIP assay was performed using histone H3 ChIP assay kits (17-245: Upstate Biotechnology) as described (34). Anti-GATA3 Ab (H-48: Santa Cruz Biotechnology) was used for precipitation. Where indicated, GFP-positive retrovirus-infected cells were sorted by flow cytometry and subjected to ChIP assay. Several primer sequences for ChIP assay were described previously (34, 42). The primer pairs newly generated are as follows: IL-5 1-F, 5′-$^{-109}$GATTGTTAGCAATTATTCATTTC^{-87}-3′; IL-5, 1-R, 5′-$^{+244}$GGTTAGGACAGCCTACCCTAC^{+224}-3′; IL-5 2-F, 5′-$^{+224}$GTAGGGTAGGCTGTCCTAACC^{+244}-3′; IL-5 2-R, 5′-$^{+646}$GATGCGGGCCATGAGCACATG^{+626}-3′; IL-5 3-F, 5′-$^{+625}$CATGTGCTCATGGCCCGCATC^{+646}-3′; IL-5 3-R, 5′-$^{+1133}$CAGGAGCTTGAGACCTAGAGAG^{+1112}-3′; IL-5 4-F, 5′-$^{+1112}$CTCTCTAGGTCTCAAGCTCCTG^{+1133}-3′; IL-5 4-R, 5′-$^{+1431}$CAACAGAGCTTATATCTCCAGC^{+1452}-3′; IL-5 5-F, 5′-$^{+1452}$GCTGGAGATATAAGCTCTGTTG^{+1431}-3′; IL-5 5-R, 5′-$^{+1795}$GAGAGGCACTAGGATGAAGAG^{+1778}-3′; IL-5 6-F, 5′-$^{+1778}$CTCTTCATCCTAGTGCCTCTC^{+1795}-3′; IL-5 6-R, 5′-$^{+2142}$CTTCAGGAACACCAGACACATAG^{+2120}-3′; IL-5 7-F, 5′-$^{+2142}$CAGATGGTTGTGAGCCAACCATCT^{+2120}-3′; IL-5 7-R, 5′-$^{+2856}$CAAGAAGCAAATAGATCAGACTG^{+2834}-3′; IL-5 8-F, 5′-$^{+2834}$CAGTCTGATCTATTTGCTTCTTG^{+2856}-3′; IL-5 8-R, 5′-$^{+3218}$CTTAAATTGTGAAGTCCTGTCAC^{+3196}-3′; IL-5 9-F, 5′-$^{+3819}$CAAGGCTTTGTGCATGTTACCAAC^{+3842}-3′; IL-5 9-R, 5′-$^{+3919}$CAGTCATGGCACAGTCTGATTC^{+3898}-3′; IL-5-RAD50 1-F, 5′-$^{-16107}$ACTTCACACTGTATGACAGTG^{-15087}-3′; IL-5-RAD50 1-R, 5′-$^{-14691}$CCTGGCTGTGAATGAATATTTGTC^{-14714}-3′; IL-5-RAD50 2-F, 5′-$^{-14336}$ACGCATTGCCCAAATCTTCAG^{-14316}-3′; IL-5-RAD50 2-R, 5′- $^{-13904}$GAAGACGGTAAGTCCTGAGGCG^{-13925}-3′; IL-5-RAD50 3-F, 5′-$^{-13698}$GAGGACCCAAAAGTTCCGAACACG^{-13672}-3′; IL-5-RAD50 3-R, 5′-$^{-13408}$TTCTAAAAGACAACAGCTACTCGT^{-13428}-3′; IL-5-RAD50 4-F, 5′-$^{-13558}$AGCAACCGTAAGCTCGCACATTCC^{-13535}-3′; IL-5-RAD50 4-R, 5′-$^{-13196}$GACTGCACCCCAGCCTACCCATGC^{-13218}-3′; IL-5-RAD50 5-F, 5′-$^{-13428}$ACGAGTAGCTGTTGTCTTTTAGAA^{-13408}-3′; IL-5-RAD50 5-R, 5′-$^{-13039}$TCACGTGATCAAGAGAAACTACTC^{-13062}-3′; IL-5-RAD50 6-F, 5′-$^{-13218}$GCATGGGTAGGCTGGGGTGCAGTC^{-13196}-3′; IL-5-RAD50 6-R, 5′-$^{-12840}$GACAATCTGCAAGAGCAAGTGCTC^{-12862}-3′; IL-5-RAD50 7-F, 5′-$^{-11433}$CGGAGGATAATTCTCCTTAAAAGG^{-11410}-3′; IL-5-RAD50 7-R, 5′-$^{-11067}$GACAAGGTCTCATTGTAGCTGTGG^{-11090}-3′; IL-5-RAD50 8-F, 5′-$^{-9305}$GCTACATAATGAGTAACCAGCTTG^{-9282}-3′; IL-5-RAD50 8-R, 5′-$^{-8923}$GAGCTGGTGCAGACCTTGTTGCCAC^{-8947}-3′; IL-5-RAD50 9-F, 5′-$^{-7140}$GAGCTGGAAGGTAAAAGGTTAGAATAG $^{-7114}$-3′; IL-5-RAD50 9-R, 5′-$^{-6761}$GAATCTTCAAGGATTGGTGACTATACC $^{-6787}$-3′; L-5-RAD50 10-F, 5′-$^{-3626}$GATTCAGGGAAACAATCTGTGGATG $^{-3612}$-3′; IL-5-RAD50 10-R, 5′- $^{-3300}$GGGTTTATGTGTTCACCATGGACC^{-3323}-3′; IL-5-RAD50 11-F, 5′-$^{-938}$CCTGCACTTTTTGTCATAGGAACC^{-915}-3′; IL-5-RAD50 11-R, 5′-$^{-556}$GTGGTGGTACACACCAGCAGATGTG^{-580}-3′; IL-5-RAD50 14-F, 5′-$^{+3172}$AGGCTGAGGCTGAGCTGCTCCATG^{+3195}-3′; IL-5-RAD50 14-R, 5′-$^{+3549}$TAACTCAGTTGGTAACATGCACAA^{+3526}-3′. The numbers indicate positions relative to the first nucleotide of the IL-5 exon 1, which is designated as +1. The primer pairs for IL-5-RAD50 12 and 13 in Fig. 6 are the same as those for IL-5 promoter and IL-5 intron, respectively.

ELISA—CD4 T cells were cultured for 7 days as described above and restimulated with immobilized anti-TCR mAb (H57-597, 3 μg/ml) for 8 h. The concentrations of IL-5, IL-4, IL-13, and IFNγ in the supernatant were determined by ELISA as described previously (42).

Retroviral Vectors and Infection—pMX-IRES-GFP plasmid was kindly provided by Toshio Kitamura (The University of Tokyo, Tokyo, Japan). The methods for the generation of virus supernatant and CD4 T cell infection were described previously (32). Infected cells were subjected to intracellular staining with anti-IL-4, anti-IL-5, and anti-IFNγ mAb or to cell sorting. A mutant of IκBα, IκBαM, was generated from the IκBα dominant-negative Vector (Mercury). cDNA for human IκBαM or human GATA3 were inserted into a multicloning site of pMX-IRES-GFP.

Immunoblot Analysis—Immunoblot analysis for GATA3, IκBα, and tubulin-α was performed as previously described (42). For IκBα, a rabbit polyclonal Ab (anti-IκBα; Cell Signaling Technology 9242) was used.

RT-PCR—Total RNA was isolated from cultured cells using the TRIzol reagent. Reverse transcription was carried out with Superscript II RT (Invitrogen). 3-Fold serial dilutions of template cDNA were performed. PCR reaction with specific primers was done as described previously (34). New primers used were GATA3 exon 1b forward, CTTTGCGGGATAGTTTAGCAA-3′, and GATA3 exon 1b reverse, 5′-GAA-